Reversible structural phase transitions in semiconductor and metal/semiconductor surfaces

2002 J. Phys.: Condens. Matter 14 6005

(http://iopscience.iop.org/0953-8984/14/24/308)

INSTITUTE OF PHYSICS PUBLISHING JOURNAL OF PHYSICS: CONDENSED MATTER

J. Phys.: Condens. Matter **14** (2002) 6005–6035 PII: S0953-8984(02)37442-3

Reversible structural phase transitions in semiconductor and metal/semiconductor surfaces

Arantzazu Mascaraque and Enrique G Michel

Departamento de Física de la Materia Condensada and Instituto Universitario de Ciencia de Materiales 'Nicolás Cabrera', Universidad Autónoma de Madrid, 28049 Madrid, Spain

Received 27 May 2002
Published 31 May 2002
Online at stacks.iop.org/JPhysCM/14/6005

Abstract

We review our current understanding of the reversible phase transitions found in clean semiconductor and metal/semiconductor surfaces. The most important phase transitions are considered in detail, in particular those appearing in Si(001), Ge(001), Si(111), Ge(111), 3C-SiC(001), Pb and Sn on Si(111) and Ge(111), Au/Si(111) and Ag/Si(111). Special emphasis is placed on recent experiments and theoretical models, as well as on open or controversial aspects of these interesting surface systems.

(Some figures in this article are in colour only in the electronic version)

1. Introduction

Surface reconstructions and phase transitions are widely investigated topics, both from theoretical and experimental points of view [1–3]. One reason for this interest is the idea that the critical behaviour of a system should depend only on very general properties, such as its spatial dimensionality and the symmetries of the phases involved. Since a phase transition is a change of order in a system, it is determined by a delicate balance between energy (U) and entropy (S), the free energy $F = U - TS$ being the relevant thermodynamic potential [1]. In the case of two dimensions (2D), the reduced dimensionality plays a very important role, because the connectivity of a system increases with dimensionality, and thus the role of entropy (through fluctuations) is less important in 3D. In one dimension (1D), each atom has only two neighbours, but this number is larger in 2D and even more in three dimensions (3D). A broad rule of thumb establishes that entropy effects are so important in 1D that no ordered states are possible for $T > 0$, while in 3D there are many interconnections to stabilize long-range order, so almost all phase transitions are of first order. The case of 2D becomes interesting because fluctuations play a much more important role than in 3D, but continuous phase transitions (second order) are frequent. On the other hand, the wide range of adsorbate/substrate systems available, exhibiting many different symmetries, interaction strengths and dimensionalities, makes it possible to access almost all the universality classes [4]. Furthermore, the different microscopic mechanisms behind the phase transition can be well analysed in this wide playground, helping

in developing theories than can be applied to 3D systems. A high degree of order is a crucial feature needed for an adequate experimental characterization of a phase transition in a surface system. The presence of defects such as vacancies or interdiffused substrate atoms is common in adsorbate systems. Such inhomogeneities can affect strongly the critical properties of the phase transition, and even mask some of its features. There are several examples in the literature where the role of defects has been analysed in detail [5–8].

Semiconductor surfaces are ideal substrates for obtaining high-quality interfaces with a reduced defect concentration. On the one hand, high-quality semiconductor surfaces can be prepared with extremely low levels of impurities and point defects. Furthermore, many different kinds of adsorbate-induced long-range-ordered superstructures with different symmetry can be prepared on these surfaces. On the other hand, the study of the phase transitions of semiconductor and metal/semiconductor surfaces is also interesting because of the more localized nature of the semiconductor bonds, as compared to the case for metallic surfaces, that have been studied to a much larger extent.

In this article the properties of the most important semiconductor and metal/semiconductor interfaces exhibiting a reversible surface phase transition will be reviewed.

2. Clean surfaces

In contrast to the case for metals, there are very few reversible surface phase transitions for clean semiconductor surfaces—limited to silicon, germanium and SiC only [9–14]. The most studied case is the reversible phase transition, occurring on going from low temperature (LT) to room temperature (RT), from c(4 × 2) to (2 ×1) reconstructions observed for Si(100) and Ge(100) surfaces. This phase transition was shown to result from switching between anticorrelated to correlated asymmetric dimers [10–13]. Other important examples of reversible order–disorder phase transitions are those from (7 × 7) to (1 × 1) and from c(2 × 8) to (1 × 1) in Si(111) and Ge(111) surfaces, respectively. A second phase transition from (2 × 1) to (1 × 1) for Si(001) and Ge(001) surfaces occurs at elevated temperatures [15]. In the case of β-SiC(100), a phase transition has been reported from a c(4 × 2) phase at RT to a (2 × 1) at high temperature [14].

2.1. The (2 × 1) ↔ (1 × 1) phase transition of Si(001) and Ge(001)

The (001) surfaces of Si and Ge exhibit a reversible (2 × 1) ↔ (1 × 1) phase transition at high temperature. In the case of Ge, surface x-ray diffraction experiments determined a transition temperature of $T_c = 955 \pm 7$ K [15]. The phase transition has been interpreted as being due to the creation of adatoms and vacancies on the surface with consequent break-up of surface dimers. It has been shown that a concomitant loss of height–height correlation takes place at the surface.

2.2. The c(4 × 2) ↔ (2 × 1) phase transition of Si(001) and Ge(001)

The phase diagrams of Si and Ge low-index surfaces have been the subject of several studies. They exhibit various phase transitions where the structural changes are accompanied by important electronic effects, such as surface metallization [16–21], rehybridization [22, 23] and bond breaking [24].

The (001) surfaces of these semiconductors are mainly characterized by a (2 × 1) surface reconstruction where the atoms of the outermost layer couple in pairs to form dimers along the $[01\bar{1}]$ direction (figure 1). The driving force for this reconstruction is a bond formation to saturate the two dangling bonds per surface atom of the ideally bulk-truncated surface. The en-

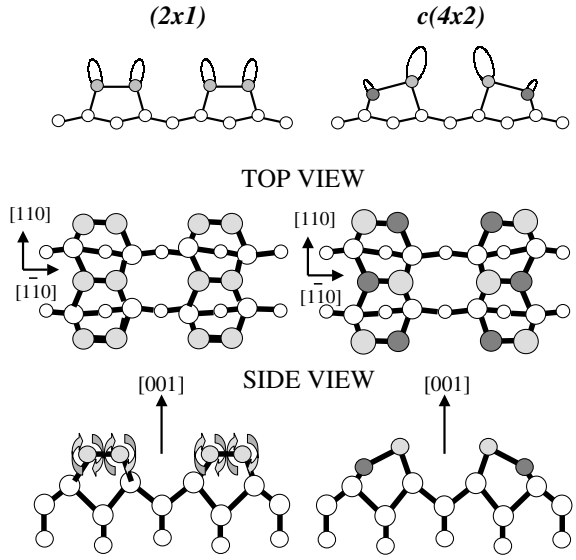

Figure 1. Schematic representations of a top and a lateral view of both the (2×1) and $c(4 \times 2)$ reconstructions of the Si(001) and Ge(001) surfaces. The figure shows the dimer formation. Arrows indicate atomic fluctuations from positions with different heights.

ergies involved in this primary reconstruction are quite strong ($\sim$1.7 eV). The reconstruction is very stable as the formation of the bond only requires a few per cent deformation of the bulk bond length [25]. Further energy reduction is achieved via dimer buckling so dimers are formed by inequivalent atoms (up and down). At LT, adjacent dimers have opposite buckling orientation and are ordered in parallel rows, thus displaying a $c(4 \times 2)$ symmetry [17]. Since dimers are spatially separated, the interactions forming the long-range ordering are weaker ($\sim$100 meV). This energy scale implies that the observed superstructures should be more sensitive to minor energy differences, due to temperature or surface preparation method.

In spite of the apparent simplicity of the reconstruction, the origin and nature of dimer structures on the (001) surface have been among the most intensively discussed issues in semiconductor surface physics. At RT, two models, with symmetric and asymmetric dimers, were under discussion until 1993, when the Si(001) symmetric dimer model was discarded in favour of the asymmetric model [13, 26–28]. The controversy had its origin in opposite results obtained with different experimental techniques and theoretical calculations, together with the experimental difficulty of preparing a well-ordered surface. RT STM topographic images found symmetric dimers on a defect-free Si(001) surface, while asymmetric dimers were associated with defects [29, 30]. Angle-resolved photoemission data were not conclusive [31]. Early energy-minimization calculations showed that buckled dimers were more stable [32], although total-energy calculations indicated that symmetric and asymmetric models had very similar energies at RT [33]. Ihm *et al* [25] performed total-energy calculations combined with position-space renormalization-group calculations to obtain predictions of the structural phase transitions of the Si(100) surface as a function of temperature. They proposed that the (2×1) reconstruction was not the ground state of the system, and that higher-order structures should appear at LT ($c(4 \times 2)$ or $p(2 \times 2)$). They predicted an order–disorder phase transition in both Si and Ge surfaces as the origin of the disappearance of the higher-order diffraction peaks in the LEED pattern at $\sim$200 K. This transition would have its origin in the disorder produced by thermal flipping motion between the two possible tilted positions.

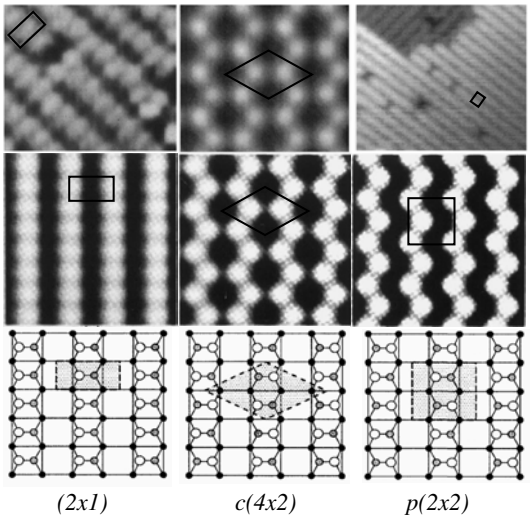

Figure 2. Top: experimental STM topographic images of the Si(001) surface taken at RT (left) and LT (centre and right). The middle panels are representations of the calculated charge-density images for the three reconstructions. White symbols indicate the unit cells. Bottom: corresponding top views of hard-ball schematic unit cells (from [29, 36, 38]).

The $(2 \times 1) \leftrightarrow c(4 \times 2)$ transition in Si(001) was first observed by means of LEED [34]. It appeared to be a reversible second-order phase transition, occurring over a wide temperature range [34]. A similar transition was also observed by means of LEED in Ge(001) [16]. Upon heating, the Ge(001) surface reversibly transforms into a (2×1) phase at $\sim$220 K [17]. This phase transition is a two-stage transition and it is much sharper than for Si(001). The existence of a $(2 \times 1) \leftrightarrow c(4 \times 2)$ phase transition confirms that the surface reconstruction is due to asymmetric dimers, as no symmetric dimer arrangement can describe the $c(4 \times 2)$ structure.

Recent experiments have shown that the (001) surfaces are even more complicated. LT STM data show symmetric dimers on Si(001) surfaces at $\sim$20 K. Asymmetric dimers are observed only near defects [35]. First-principles calculations have predicted that the $p(2 \times 2)$ configuration is also stable for the Si(001) surface at 0 K [36]. This structure consists in an out-of-phase and in-phase ordering of the buckled dimers along and perpendicular to the dimer rows, respectively (see figure 2). The $c(4 \times 2)$ and $p(2 \times 2)$ reconstructions are interchangeable by simple dimer inversion (see figure 2), while other phases (such as $c(2 \times 2)$) cannot be created without breaking dimer bonds. Both $c(4 \times 2)$ and $p(2 \times 2)$ have been locally detected by STM over a wide temperature range and they are related to the presence of steps, vacancies or defects. This could be understood as an indication that the ground state of the Si(001) surface is not $c(4 \times 2)$, but a symmetric structure at the zero-temperature limit, and that the intermediate $c(4 \times 2)$ is always related to some kind of defect. The calculated total energies of the $c(4 \times 2)$ and $p(2 \times 2)$ structures are very similar (the energy difference is only $\sim$12 meV/dimer) [37–40]. It is not possible to resolve the energy difference without improving the accuracy of the best calculations. Thus the ground state configuration of this surface is still controversial.

A possible scenario for the reconstruction of Si(001) surfaces is the following. The symmetric dimers are stabilized at LT because of an antiferromagnetic coupling between dimers. With increasing temperature, the antiferromagnetic order is thermally destroyed and then asymmetric dimers become more stable than symmetric ones. A further increase of temperature (above 100 K) leads to thermal excitations that include moving phase defects,

which change the phase of the asymmetry [41]. Again, apparently symmetric dimers dominate the surface at RT.

The difference in behaviour between Si and Ge surfaces can be rationalized on the basis of chemical arguments. The reconstruction energy per surface unit cell in (001) surfaces comes essentially from the formation of a new bond, and it follows the same trend as the cohesive energy per bulk bond. The energy gain due to asymmetric compared to symmetric dimer formation is 0.14 eV in Si as versus 0.40 eV in Ge [42]. As a consequence, at RT the dynamical dimer flipping is 1000 times larger in Si than in Ge, where the flipping is quite suppressed. In spite of this distinction, the two phase transitions exhibit similar features and they can be described within the same framework.

2.2.1. Nature of the order–disorder phase transition. *Ab initio* calculations predict that the (2×1) reconstruction is not stable. Starting from a (2×1) geometry and relaxing ions and electrons in order to achieve structurally optimized parameters, dimers tilt in such a way as to produce a higher-order reconstruction [43, 44]. Flipping movements of dimers has been detected from a theoretical dynamical evolution analysis. An examination of the time evolution has shown that dimers along a row tend to flip simultaneously and impart to the system a long-range $c(4 \times 2)$ order [36]. Dimers along a row exhibit strong correlation, that is reduced between the rows. It is widely accepted that the flipping of single dimers is the elementary excitation in the disordered phase. These vertical movements freeze as temperature decreases, leading to an ordered $c(4 \times 2)$ reconstruction.

The phase transition was first simulated by a Monte Carlo method by Saxena *et al* [45], using an asymmetric dimer model representing the Ising system. The analogy with an Ising magnet is simple: a dimer corresponds to a localized spin that has a uniaxial orientation. As dimers are aligned, the (2×1) reconstruction represents the ferromagnetic case. The $c(4 \times 2)$ structure is the antiferromagnetic case, since nearest-neighbour dimers are oriented oppositely. At LT the surface consists in $c(4 \times 2)$ domains formed by asymmetric dimers. As the temperature is increased, XRD data have proved that, although domain size decreases, the total number of buckled dimers remains constant [46]. This implies that the (2×1) reconstruction consists in a random distribution of asymmetric dimers. Consequently, the transition can be described as an order–disorder phase transition.

A simple 2D Ising model cannot fully describe the temperature dependence of the streaks in the LEED pattern [47], a clear indication that the phase transition is more complex than originally expected. The presence of streaks associated with the $c(4 \times 2)$ structure, even at temperatures twice as high as T_c, indicates a strong short-range order along the dimer row. As shown in figure 3, the temperature evolution of the Si(001) LEED diffraction spots deviates from Onsager's thermodynamic formula, suggesting that more complex effects have to be considered. Indeed, in order to reproduce the experimental data, the influence of the second-layer displacement to the classical dipole–dipole interaction has to be added. This fact is also supported by core-level photoemission data. The spectra measured at RT and LT for the (2×1) and $c(4 \times 2)$ reconstructions have shown a close similarity. However, layers underneath influence the lineshape, indicating that the reconstruction is affected by a subsurface transformation [26]. This second-layer influence can be understood if we notice that the LEED streak pattern is only obtained when a strong anisotropy is introduced in the 2D Ising system: the interaction within a dimer row should be much stronger than the coupling between dimer rows. The antiferromagnetic ordering is then obtained by an alternating displacement of the second-layer atoms along the dimer row.

However, although an anisotropic coupling reproduces the streak pattern, the sigmoidal change of the intensity of the diffraction spots observed in figure 3 cannot be explained by this

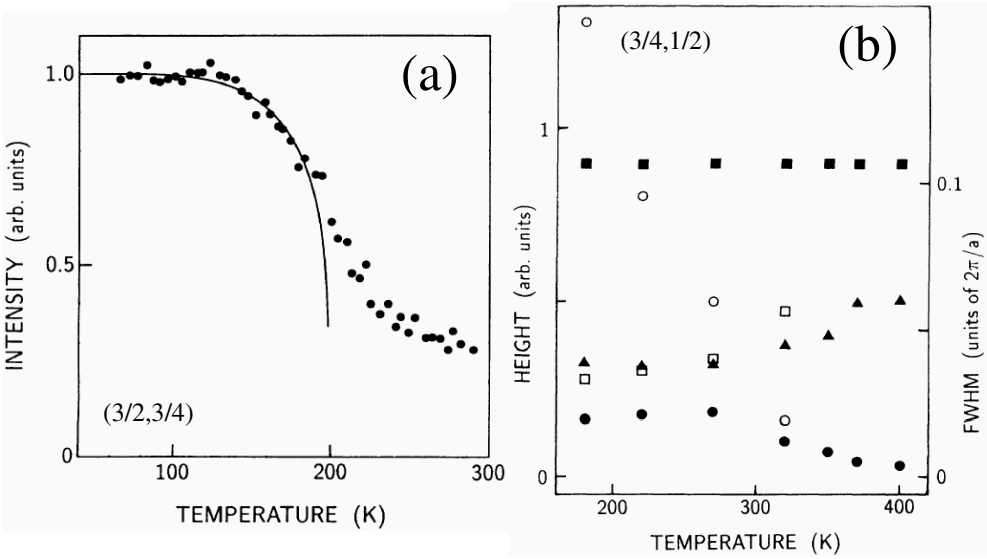

Figure 3. (a) The temperature evolution of the intensity of the (3/2, 3/4) diffraction spot during the phase transition. The solid curve correspond to Onsager's formula. (b) The temperature dependence of the width (triangles), length (squares) and height (circles). Open symbols come from the (3/4, 1/2) diffraction peak, while closed ones correspond to streak data (from [47]).

effect alone. In order to reproduce this behaviour the role of defects has to be considered. On the Si(001) surface, dimer vacancies are spontaneously produced, and it is known from early experiments that even a very small content of vacancies affects the transition [48]. In fact, a surface with a high density of defects exhibits no phase transition, due to the energy reduction that a vacancy generates by reducing the number of dangling bonds. The finite size of the domains (connected to dimer vacancies) manifests itself in several effects, such as the tail effect of the temperature dependence of the (3/2, 3/4) diffraction spot [49].

The presence of defects affects also the sharpness of the phase transition. From the theoretical order parameter behaviour, it is deduced that the phase transition should be very sharp [37]. However, the experimental LEED intensity evolution shows a broad transition range around the transition temperature. This is due to the presence of an intrinsic small content of surface defects. It is reliably found that just a 1% content of defects reduces the order parameter by 75%, leading to a diffuse transition. This change can be easily explained by the fact that the presence of defects is equivalent to a spin Ising model with a random magnetic field, and that a long-range magnetic field is destroyed by a random magnetic field [48]. However, at RT the average separation of defects becomes similar to the dimer correlation length, so defects start to play no significant role in the average properties [37].

The analysis of the SXRD data shows again the strong influence of the defects together with the important effects of the anisotropic interaction. Figure 4 represents the temperature dependence of the width and the intensity of the diffraction reflection spots for the Ge(001) surface [46]. The difference between the two widths (parallel and perpendicular to dimer rows respectively) indicates that the domains are much larger along the dimer row direction than in the perpendicular direction. The c(4 $\times$ 2) unit cell has two different domains, related to each other by a $2a$-translation vector along the [110] direction. Therefore, the reconstruction can have an antiphase domain structure within a single terrace. As can be observed, domain

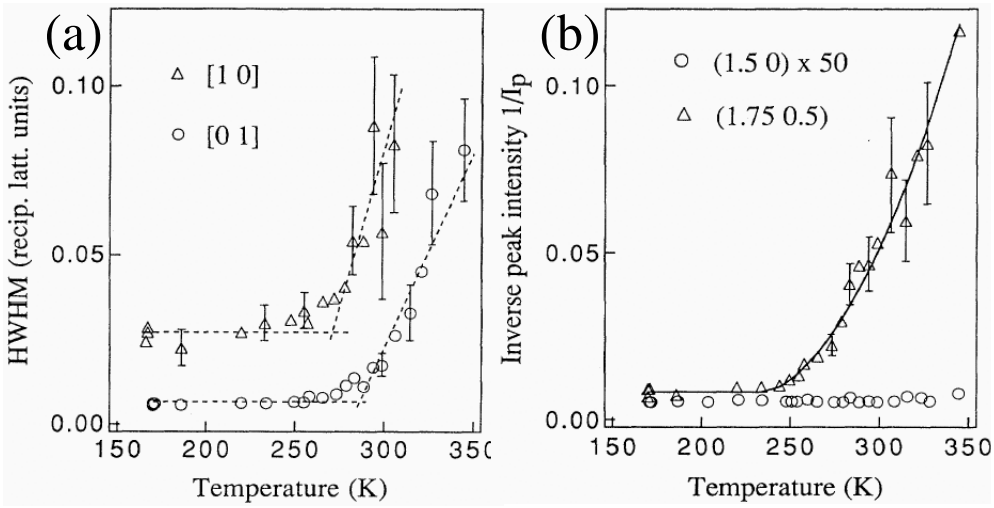

Figure 4. (a) The temperature dependence of the HWHM of the (7/4, 1/2) diffraction peak during the phase transition. Circles and triangles correspond to cuts along the [01] and [10] directions, respectively. Dashed lines are only a guide to the eye. (b) The temperature evolution of the inverse of the intensity for (7/4, 1/2) (triangles) and (3/2, 0) (circles) diffraction peaks. The sharp increase at ∼250 K is an indication of the phase transition (from [46]).

sizes saturate, probably due to the pinning by defects of antiphase domains. The temperature evolutions of the two widths are similar at the beginning of the transition, and the difference in slope of the curves indicates again that the interaction is much stronger within rows than between rows. This anisotropy is larger in this surface than for Si, and this should be why the transition appears to be a two-stage phase transition for Ge.

2.2.2. Critical exponents. The pinning by defects of the c(4 × 2) domains saturates the domain size, and prevents the observation of universal critical behaviour of the Ge(001) phase transition [50]. STM measurements have shown that in the Si(001) case, the surface has typically more defects, so the critical behaviour related to the phase transition in Si(001) should be extremely difficult to observe.

The second-order transitions between the ferromagnetic and the antiferromagnetic phases belong to the 2D Ising universality class. For this class, the correlation length (ν) and the order parameter (β) should be 1 and 1/8 respectively. While agreement on the order/disorder nature of the transition is well established, a clear assignment to the 2D Ising class is still controversial. The first measurements of the order parameter critical exponent β by means of LEED gave the 1/8 Ising value [51], but XRD experiments found $\beta = 1/2$, a value much closer to the mean-field prediction [52]. Similar attempts to study the correlation length of the order parameter fluctuations failed to determine the corresponding critical exponent ν, for both Ge(001) [46] and Si(001) [47], possibly due to the influence of defects [37, 53]. This strong influence is represented in figure 5, where it is clearly apparent that they affect the temperature evolution of the order parameter across the phase transition. A more recent analysis based on He beam diffraction has determined the critical exponents $\nu = 1.1 \pm 0.2$ and $2\beta = 0.24 \pm 0.02$, from the measurements of the (1/2, 1/4) peak intensity and width [50] (see figure 6). These values fall within the 2D Ising universality class (see figure 6).

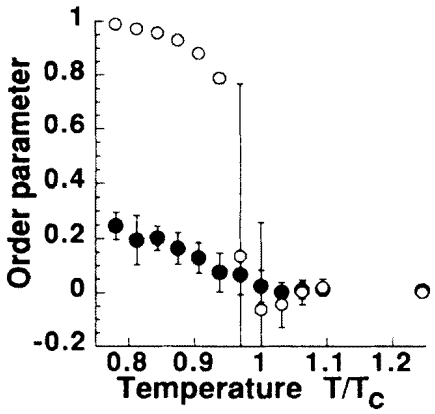

Figure 5. The temperature evolution of the theoretical order parameter of the Ge(001) c(4 × 2) ↔ (2 × 1) phase transition. Open circles correspond to a defect-free surface, while closed circles were obtained for a surface with a 1% defect content. Notice the dramatic influence of the defects on the nature of the phase transition (from [37]).

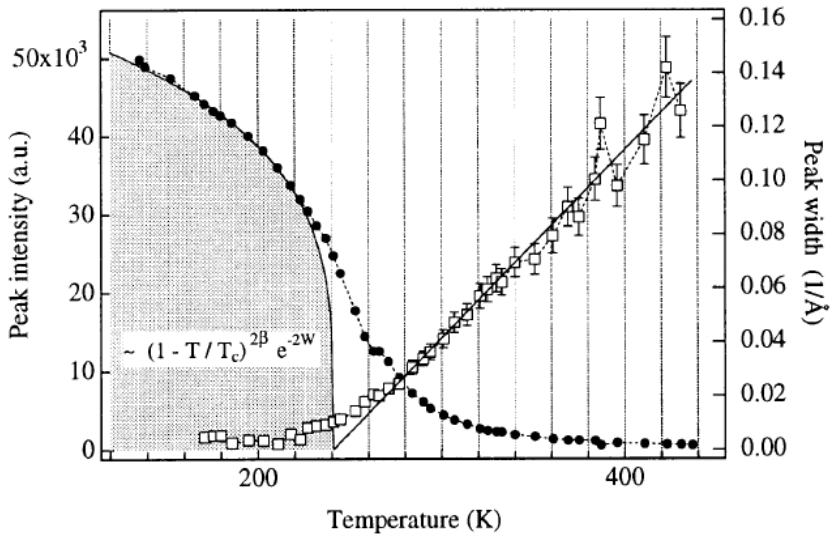

Figure 6. The temperature dependence of the intensity and the width of the (1/2, 1/4) diffraction peak. The extrapolation to zero of the peak width (open squares) leads to the critical temperature of the phase transition. This value, together with the analysis of the intensity (solid circles), allows the determination of the critical exponent β (from [46]).

2.2.3. Driving force for ordering. As mentioned above, a short-range interaction is responsible for the dimer bond formation. Two possible driving forces can be suggested as the origin of the dimer ordering at LT: a long-range Fermi surface instability [54] or a short-range dimer coupling [16]. In the first case, a surface band should cross the Fermi level at RT with a $\vec{k}_{\parallel}$-vector characteristic of the reconstructed surface $\vec{q}$-periodicity. This mechanism involves band-structure effects and it is a long-range interaction. Alternatively, a similar mechanism for dimer creation could drive the formation of the c(4 × 2): a weak interaction between nearest dimers through d electrons, which would be a short-range interaction.

In Ge(001), the phase transition takes place in two stages: first, an ordering along a dimer

row; and second, one perpendicular to it [17]. This is an indication that the interaction has an strong angular distribution anisotropy. In addition, real-space calculations have proved that the lowest elementary excitation of the system is a simple dimer flip, and that collective dimer motion is not important [25]. Also, only a non-dispersive band has been detected in the centre of the SBZ [17]. All this evidence supports the notion that the driving force responsible for dimer ordering is a short-range neighbour dimer coupling.

We can summarize the plentiful experimental and theoretical information available by saying that the (001) Si and Ge surfaces are characterized by a short-range reconstruction, combined with a weak long-range ordering. From experimental and theoretical studies, it is well established that the basic reconstruction mechanism consists in the formation of buckled dimers, and the (2×1) structure at RT is due to thermally activated flip-flop motion of the buckled dimers between their two possible orientations. At temperatures below $T_c \sim 200$ K, the (2×1) structure is transformed into the $c(4 \times 2)$ structure. The LT structure results from an antiphase ordering of the buckled dimers. The transformation is described as an order–disorder phase transition with respect to the dimer buckling, and the phase transition behaviour has been characterized as an Ising spin model. Except for some properties related to the chemical origin (bond strength, density of defects etc), the two phase transitions are essentially identical and can be described within the same framework.

2.3. The $(7 \times 7) \leftrightarrow (1 \times 1)$ *phase transition of Si(111)*

The Si(111) surface is one of the most studied systems in surface science. The stable structure at RT is the (7×7) reconstruction, that is due to a complex surface reordering described in the dimer–adatom–stacking fault (DAS) model [55]. At temperatures higher than ∼1100 K the surface reverts to a (1×1) phase [56]. This phase transition was soon characterized using different techniques [57–59]. A monitoring of the phase transition by using low-energy electron diffraction (LEED) [56, 58, 60] and reflection high-energy electron diffraction (RHEED) [61, 62] showed that the (7×7) superlattice spots disappear gradually over a broad temperature range (∼50 K). This finding was confirmed later on [63] and suggested that the phase transition is second order. This would be in disagreement with the predictions of Landau symmetry rules [64–66]. The controversy was solved by reflection electron microscopy (REM) [59, 67], low-energy electron reflection microscopy [68, 69] and scanning tunnelling microscopy (STM) [70]. These techniques showed the coexistence of (1×1) and (7×7) domains during the transition, a typical feature of a first-order phase transition. Figure 7 shows the appearance of (7×7) areas nucleated at the step edges of the (1×1) surface as the phase transition is crossed. In other experiments [62, 71, 72] an appreciable hysteresis was found, also in agreement with a first-order phase transition. Figure 8 shows the changes in the integrated intensity of the $(1/7, 3/7)$ superlattice reflection as a function of temperature across the phase transition. There is a significant hysteretic difference of 5 °C, but no indication of peak broadening during the phase transition. Thus, the process exhibits all the features typical of a first-order phase transformation, as also shown in He diffraction experiments [74] and RHEED [61].

There has been also some controversy as to whether the phase transition is of the order–disorder type or not. The nature of the transition can only be clarified when the structure of the (1×1) phase is known. Early reports [57] found residual $(\sqrt{3} \times \sqrt{3})$R30° periodicity in the RHEED pattern of the (1×1) phase, which was also observed in LEED [73]. This is an indication of a surface structure more complex than a simple (1×1) bulk-like atomic arrangement, but He diffraction experiments suggested that the phase transition could be of the order–disorder type [74]. Early studies [61] proposed a structural model for the (1×1)

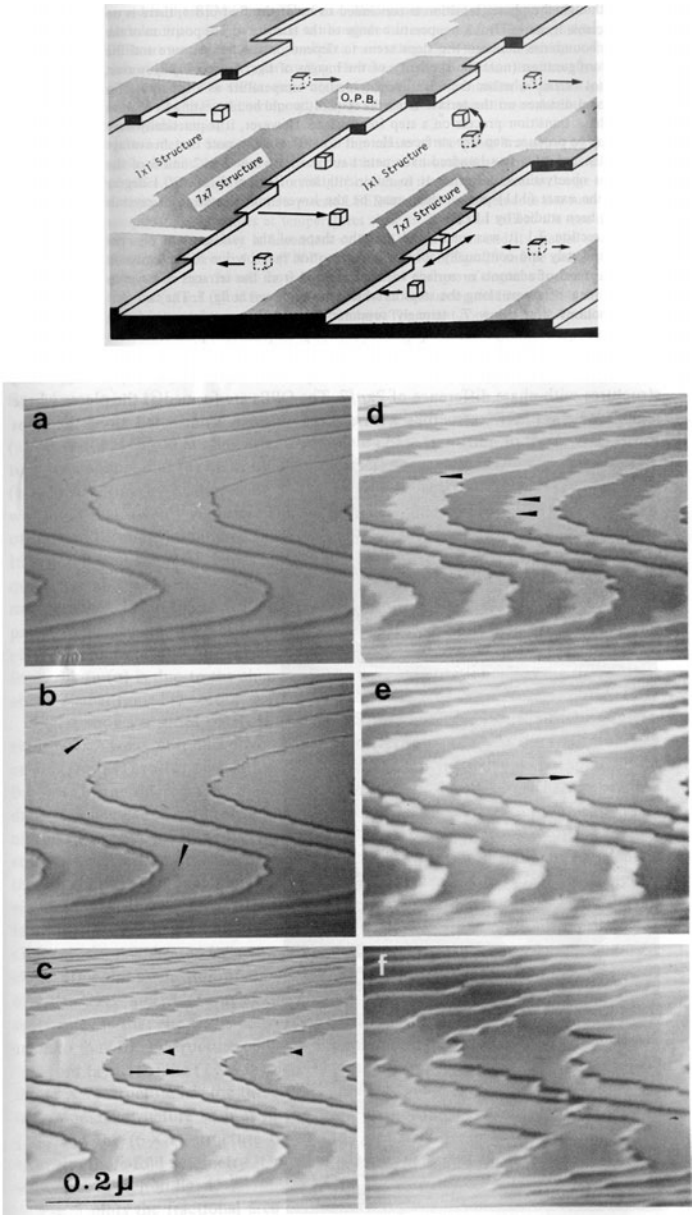

Figure 7. Bottom: reflection electron micrographs of the $(1 \times 1) \leftrightarrow (7 \times 7)$ transition (upon cooling) for a stepped Si(111) surface: (a) initial (1×1) structure; (b)–(e) (dark) regions of (7×7) nucleate at the top of monatomic steps and expand across the terraces (full arrows in (c) and (e) indicate the direction of growth); (f) completed (7×7) structure. Top: a schematic representation of the growth process (OPB denotes an out-of-phase domain boundary) (from [59]).

phase different from a simple disorder of the (7×7) structure, with adatoms randomly distributed over a relaxed bulk-like surface. The presence of adatoms was confirmed from REM measurements [59, 67], that revealed a significant role of atomic steps in the transition, and more recently by STM [75]. Indeed, the upper step edges act as nucleation centres for the

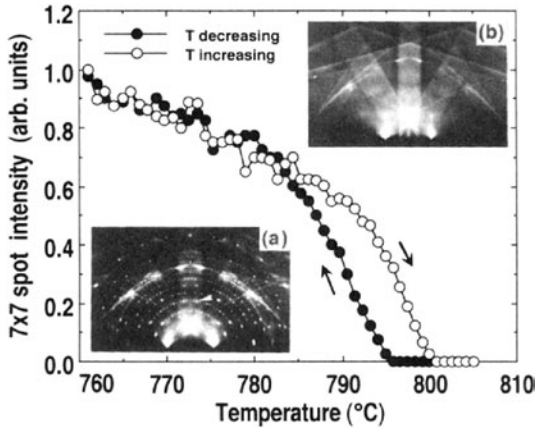

Figure 8. The integrated intensity of the (1/7, 3/7) superlattice RHEED spot from a clean Si(111)-(7 × 7) surface as a function of temperature. The hysteresis between the T-decreasing and T-increasing curves is typical of a first-order phase transition. The RHEED patterns of a (7 × 7) phase at RT and a (1 × 1) phase at 1082 K are inserted (from [62]).

(7 × 7) phase [59, 76, 77]. Some more information on the nature of the (1 × 1) phase has been gained recently. It has been established that the reconstruction is due to a gas of up to 0.20–0.25 ML of adatoms (1 ML = 7.8×10^{14} cm^{-2}) preferentially occupying the T_4 sites of a bulk-like surface [61, 67, 72, 73, 78, 79].

An additional interesting question is that of the nature of the (1 × 1) phase up to melting. Recent RHEED experiments have shown [80] that the coverage of the (1 × 1) structure is 0.25 ML in the temperature range between 1230 and 1440 K. Around 1530 K, the surface structure transforms to a new phase, with a reduced adatom coverage (0.20 ML). At 1570 K, another phase transition occurs on the surface, and a surface melting layer of 0.65 ML is formed above 1620 K. The crystalline structure below the liquid-like phase is a vacancy structure, where all adatoms, 35% of the first-layer atoms and 10% of the second-layer atoms are missing.

2.4. The phase transitions of Ge(111)

The stable reconstruction of a clean Ge(111) surface at RT is c(2 × 8) [81–83]. The reconstruction is due to the ordering of 0.25 ML of adatoms that occupy T_4 sites of a bulk-like-terminated (111) surface [84, 85]. The first phase transition is observed at 573 K, when the surface reversibly changes into a (1 × 1) pattern. A second phase transition to a second (1 × 1) structure is observed at 1050 K [60].

We consider first the phase transition at 570 K. Since the symmetry of the c(2 × 8) reconstruction allows three different orientations of the unit cell on the (111)-like substrate, three domains are observed both in the LEED and in the STM experiments [83, 86]. Disordered regions grow from the domain boundaries as the temperature approaches ∼573 K [85], when the whole adatom layer is disordered into an apparent (1 × 1) LEED pattern [69]. The disorder occurs by diffusion of surface atoms in the $\langle 01\bar{1} \rangle$ directions. An analysis of the Ge 3d core level across the phase transition [86, 87] shows that no changes occur in either the binding energies or the relative intensities of the different surface components. Since core-level spectroscopy is a local probe, this was interpreted as typical of an order–disorder phase transition. This idea was supported by ellipsometry measurements [88]. The dynamics of the phase transition has been investigated by means of time-resolved RHEED [89]. It was concluded that the adatoms

of the c(2 × 8) structure start to disorder at ∼510 K and give rise to a disordered adatom arrangement at ∼573 K. In summary, the first (1 × 1) phase presents the same content of adatoms as the c(2 × 8) structure, but the long-range order of the latter is lost.

Another phase transition to a second (1 × 1) phase takes place at 1050 K [60]. Extensive experimental and theoretical studies [18, 20, 23, 90–93] have been devoted to the high-temperature Ge(111) surface, but only recently has a comprehensive model been developed [94]. One of the features that explains this interest is the observation that the high-temperature phase is metallic. Ge is a semiconductor, but it becomes metallic at high pressures and in the molten state. Thus, a metallic phase could be an indication of premelting. A first model describes the top Ge bilayer as laterally diffusive, quasi-liquid-like and metallic. This model for the high-temperature phase is supported by photoemission and photoabsorption spectroscopy experiments [90], ion scattering [91], electron-energy-loss spectroscopy [92] as well as *ab initio* molecular dynamics simulations [93]. In contrast, helium-atom scattering (HAS) diffraction experiments [20, 23] indicate that the HT surface is well ordered but exhibits a reduced surface corrugation, consistent with an ordered metallic solid state. This model agrees also with earlier x-ray diffraction data [95] and with metastable de-excitation spectroscopy experiments [96], that find also a metallized but ordered surface above the phase transition. These apparently conflicting findings have been reconciled by quasielastic and elastic He scattering experiments [94]. Diffraction peaks exhibit identical profiles and widths below and above the phase transition (see figure 9). This indicates that the top layer is also ordered above T_c, and that the phase transition is of the order–order type. The intensity of the quasielastic peak is very sensitive to surface defects. This property was used to probe the adatom density as a function of temperature. Figure 10 shows the temperature dependence of the intensity and width of the peak. It was found that the number of adatoms present at the surface increases from 25% at 1050 K to 31% at 1100 K. The abrupt increase of the peak width at T_c indicates an onset of the surface diffusion. Figure 11 shows the dependence of the peak width on the parallel momentum transfer. A continuous diffusion model would give rise to the dotted curve in figure 11, while the dashed curves are based on a jump diffusion model. The diffusion constant found is $D = (1.2 \pm 0.2) \times 10^{-4}$ cm^2 s^{-1}, i.e. comparable to the diffusion coefficient of liquid Ge. The model found for the phase transition is shown in figure 12. At RT, 0.25 ML of adatoms are regularly arranged to produce a c(2 × 8) reconstruction. At 573 K the adatoms begin to diffuse along the [10$\bar{1}$] directions [85, 97] and are arranged in a (1 × 1) structure with local (2 × 2) order. This explains the persistence of (2 × 2) spots in LEED above 573 K. The short-range 2× order decreases as temperature approaches 1050 K. Between 573 and 1050 K the diffusion is slow ($D \leqslant 10^{-9}$ cm^2 s^{-1}), and the adatoms spend most of the time at T_4 sites. At the phase transition, the number of adatoms increases up to ∼31%. Because of this, the electronic structure of the surface is modified: it becomes metallic and the surface corrugation diminishes accordingly [20, 23, 60, 95]. The diffusion barrier is now much lower ($D = (1.2 \pm 0.2) \times 10^{-4}$ cm^2 s^{-1}) and the diffusion process takes place by jumps between T_4 sites.

2.5. The c(4 × 2) ↔ (2 × 1) phase transition of β-SiC(100)

Silicon carbide (SiC) is a large-band-gap IV–IV compound semiconductor. It has received considerable attention during the last few years due to its many different advanced applications in high-temperature, high-speed and high-power devices [98]. Also, the surfaces of SiC exhibit a very interesting behaviour from a fundamental point of view. For instance, the hexagonal 6H-SiC(0001) phase seems to present a Mott–Hubbard ground state [99]; some reconstructions of the cubic 3C-SiC(001) are formed by one-dimensional atomic chains [100, 101]; and this

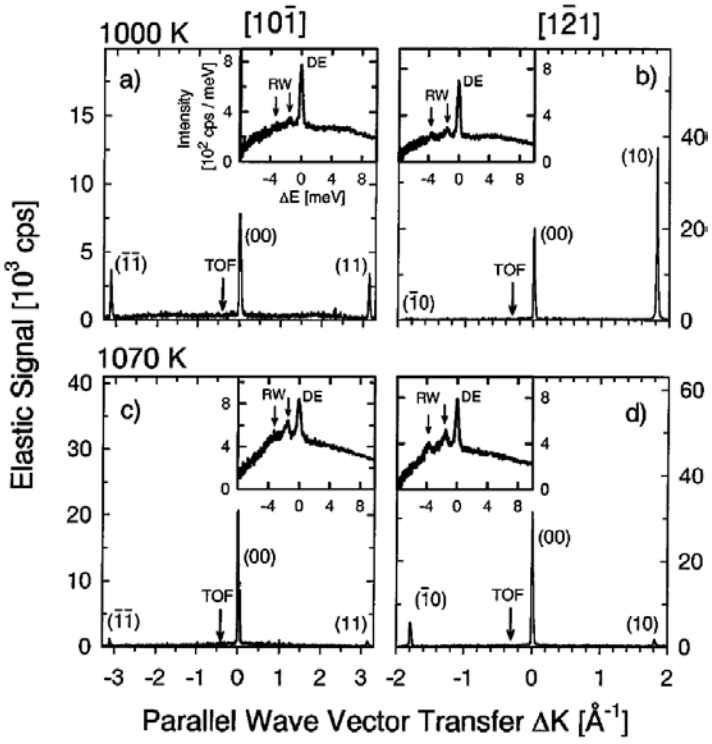

Figure 9. Angular distributions of He atoms scattered from Ge(111) along the two directions [10$\bar{1}$] ((a) and (c)) and [1$\bar{2}$1] ((b) and (d)) at temperatures directly below ((a) and (b)) and above ((c) and (d)) $T_c = 1050$ K. The insets show the corresponding TOF spectra plotted to the same scale as in (a) (from [94]).

phase also exhibits a temperature-induced phase transition between the stable c(4 × 2) RT structure [102, 103] and a high-temperature (2 × 1) phase [104]. We concentrate in the following on the properties of this phase transition.

The atomic geometry of the c(4 × 2) phase is very different when compared with the LT Si(001) and Ge(001) c(4×2) reconstructions (see [10–13] and also previous sections). It results from dimer rows having alternately up-and-down dimers (AUDD) within the row [102]. The compressive surface stress applied to Si atoms in the 3C-SiC structure plays a crucial role in the stabilization of the AUDD structure [102, 105]. Due to the difference in lattice parameters, the Si atoms are compressed by ∼20% when compared with Si(100) [106], and this is significantly reduced in the AUDD structure [107]. As temperature increases above 675 K, a (2 × 1) phase is stabilized. The phase transition is reversible and the corresponding LEED patterns correlate well with the periodicity observed in the STM pictures (see figure 13).

On the other hand, concomitantly with the structural phase transition, a semiconductor-to-metal phase transition takes place [106]. In view of the fact that all dimers are on average at the same height in the (2 × 1) phase, the origin of the electronic changes could be related to a difference in the orbital overlap. Indeed, in the (2 × 1) configuration, the distance between Si dimers belonging to the same row would be decreased to its minimum value at 3.08 Å. This would in turn significantly increase the overlap between surface atom electronic orbitals, favouring a metallic character for this surface [104]. In this model, the phase transition would be due to a change in the vertical position of the up-and-down Si dimers, either to a flat layer,

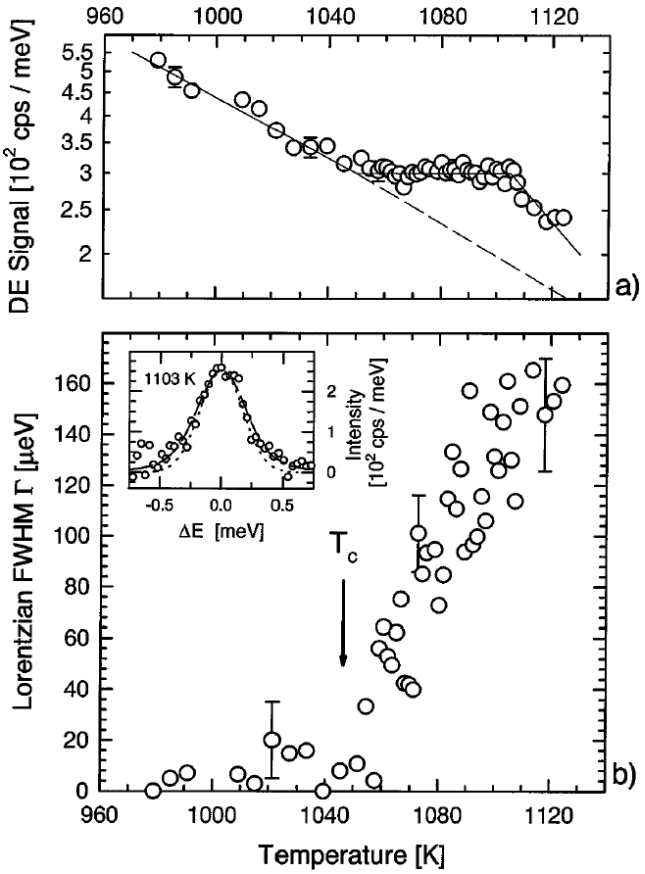

Figure 10. Temperature dependences of the intensity (a) and the Lorentzian width (b) of the quasielastic peak measured along the $[1\bar{2}1]$ direction. The inset displays the quasielastic peak measured at 1103 K. The dashed line corresponds to the apparatus response function; the solid line is a fit to the data points (Voigt curve) (from [94]).

or to a layer with dimer vibrations, but where the dimers are on average at the same height. On the other hand, the (2×1) phase exhibits interesting electronic properties, that have been attributed in part to 1D effects [104, 106]. Some more information on the structure of both phases is needed to further characterize the phase transition.

3. Metal-covered surfaces

3.1. The $(\sqrt{3} \times \sqrt{3})R30° \leftrightarrow (3 \times 3)$ *phase transition of Pb, Sn on Ge(111) and Si(111)*

A lot of attention has been attracted during the last few years by the phases formed by 0.33 ML of Pb or Sn on Ge(111) and Si(111). These phases are all ordered forming a $(\sqrt{3} \times \sqrt{3})$R30° structure at RT, but at least Pb/Ge(111), Sn/Ge(111) and Pb/Si(111) exhibit a LT phase characterized by a new (3×3) ordering [108–110]. The phase transition is reversible, and it was claimed to be due to the stabilization of a surface charge-density wave (SCDW), i.e., a periodic redistribution of charge, possibly accompanied by a small periodic lattice distortion, which determines a change of surface symmetry [108, 109]. This mechanism is well known in bulk,

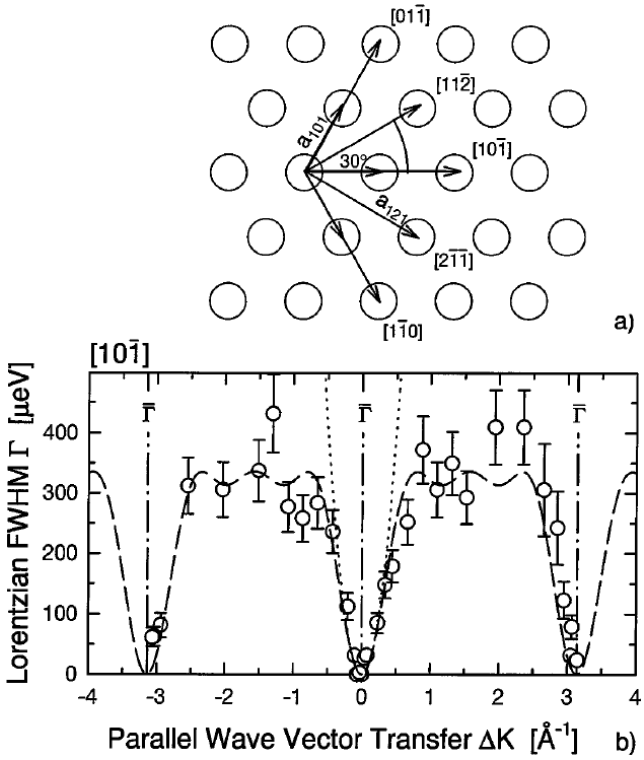

Figure 11. (a) The hexagonal lattice of the Ge(111)-(1 × 1) surface with selected jump vectors and (b) the energy broadening of the quasielastic peak as a function of ΔK along the [10$\bar{1}$] parallel direction. The dotted curves are the fits based on the continuous diffusion model, while the dashed curves are fits made for a jump diffusion model. The dot–dashed curves represent the Brillouin zone centres ($\bar{\Gamma}$) points) (from [94]).

and it has been investigated in surface systems for several years [111]. Further experiments with different techniques showed that the properties of the (3 × 3) and ($\sqrt{3} \times \sqrt{3}$)R30° models do not agree with a SCDW of this kind [112–116]. Thus, alternative models based on the existence of dynamical fluctuations [112] or on a role for defects [116, 117] were put forward. In the dynamical fluctuations model, the ($\sqrt{3} \times \sqrt{3}$)R30° phase can be understood as the result of thermal vertical disorder in the (3 × 3) phase. This point is now accepted by most authors [117], but crucial questions regarding the driving force of the phase transition and its nature (whether it is of order–disorder type or not) are not yet answered, and indeed there are contradictory reports [118, 119]. A recent theoretical study claims that the softening of a phonon is behind the formation of the (3 × 3) phase [119]. For a detailed review on these interesting system, we refer the reader to the article by Ortega *et al* [120] in this Special Issue.

3.2. The phase transitions in the Au/Si(111) interface

The deposition of Au on a Si(111) gives rise to several different surface reconstructions. Figure 14 shows a summary of the phase diagram obtained from RHEED measurements [121]. The main phases for coverages up to ∼1 ML are the (5 × 2), the α-($\sqrt{3} \times \sqrt{3}$)R30°, the β-($\sqrt{3} \times \sqrt{3}$)R30°, the (6 × 6), and the (1 × 1) phase that is observed at high temperatures. Extensive research has been carried out on the structures of these reconstructions over the

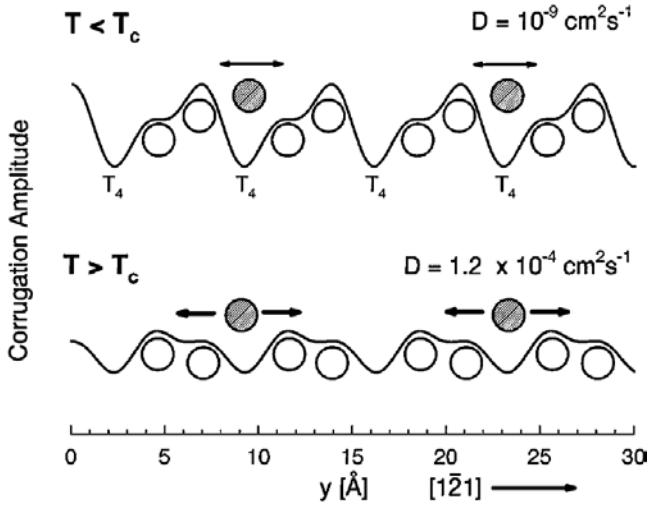

Figure 12. A schematic representation of a perpendicular cut of the Ge(111) surface along the [1$\bar{2}$1] direction at temperatures below (upper panel) and above (lower panel) $T_c = 1050$ K. Solid curves represent the corrugation functions of the top surface bilayer, open circles represent the Ge atoms in the first bilayer and shaded circles represent the Ge adatoms (from [94]).

years. While significant progress has been made, no consensus has been achieved on most of the phases. We refer the reader to [122] for an updated account on the different existing models and their features. Figure 15 shows a summary of the most important surface structures as detected by means of LEED.

In this report we will concentrate on the properties of three different phase transitions that are observed in Au/Si(111) interfaces, and that exhibit very different properties, namely the order–disorder transitions of the β-($\sqrt{3} \times \sqrt{3}$)R30° surface and that from (5 × 1) or (5 × 2) to (1 × 1), and the phase transition from α-($\sqrt{3} \times \sqrt{3}$)R30° to β-($\sqrt{3} \times \sqrt{3}$)R30° and (6 × 6) obtained by changing the coverage.

3.2.1. The order–disorder phase transition of the β-($\sqrt{3} \times \sqrt{3}$)R30° phase. At temperatures above 850 K the (5 × 2) and β-($\sqrt{3} \times \sqrt{3}$)R30° phases do not coexist with other structures. In this temperature range they were shown to undergo order–disorder phase transitions around 1070 and 1057 K, respectively. Their critical properties were analysed using spot-profile RHEED [124, 125], and they seemed quite different. An analysis of the shape of a superstructure peak across the phase transition suggested that for the (5 × 2) reconstruction the phase transition is of first order, while for the β-($\sqrt{3} \times \sqrt{3}$)R30° reconstruction, the phase transition is continuous. This assignment is in agreement with symmetry considerations, because the (5 × 2) phase should undergo a discontinuous transition, and the β-($\sqrt{3} \times \sqrt{3}$)R30° phase should belong to the three-state Potts universality class, if the transition is continuous. However, this assignment based in symmetry arguments can be very complicated if the unit cell contains more that one Au atom and substrate atoms are also involved in the phase transformation.

The β-($\sqrt{3} \times \sqrt{3}$)R30° phase appears at coverages above 1 ML and for elevated temperatures (see figure 14). In these conditions, a ($\sqrt{3} \times \sqrt{3}$)R30° ordered layer coexists with clusters of Au when the saturation coverage (1 ML) is exceeded. At elevated temperatures these islands act as Au reservoirs, and the chemical potential is controlled by temperature

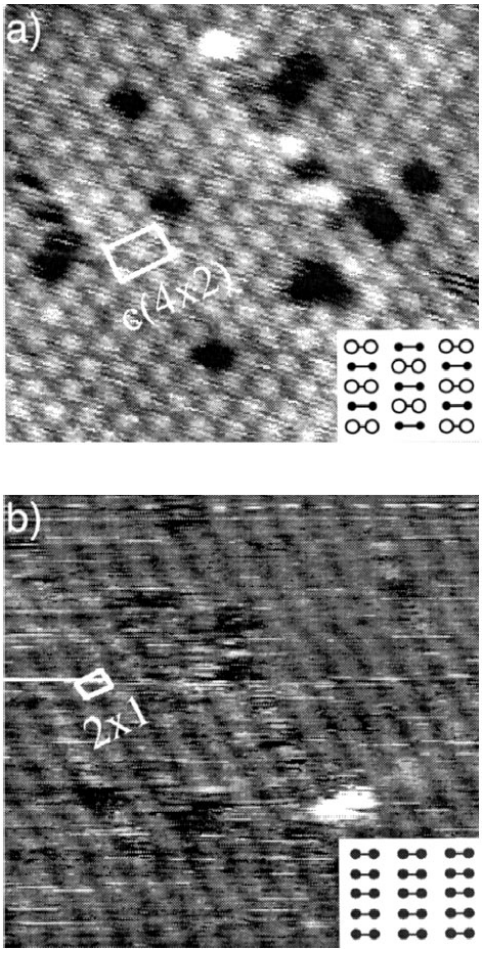

Figure 13. 100 Å × 100 Å STM topographs (filled states): (a) β-SiC(100)-c(4 × 2) at RT and (b) β-SiC(100)-(2 × 1) at 700 K. The corresponding schematic structures of dimers rows are also displayed as insets (from [106]).

only. The thermodynamic equilibrium between 3D Au islands and the 2D $(\sqrt{3} \times \sqrt{3})$R30° phase constitutes an almost unique situation for chemisorbed adsorbates. The phase transition from β-$(\sqrt{3} \times \sqrt{3})$R30° to (1 × 1) has been analysed in great detail by Nakajima *et al* [126] using spot-profile LEED (SPA-LEED). They obtained high-resolution profiles of several superstructure peaks (see figure 16). The profiles were analysed taking into account three different contributions to the lineshape $S(\boldsymbol{q}_\parallel, t)$:

$$S(\boldsymbol{q}_\parallel, t) = I_0(t)\delta(\boldsymbol{q} - \boldsymbol{q}_0) + \frac{\chi_0(t)}{1 + (\boldsymbol{q} - \boldsymbol{q}_0)_\parallel^2 \xi^2(t)} + \text{bg}. \tag{1}$$

The first term describes the contribution from long-range order. For a continuous phase transition it behaves as $I_0(t) \propto |t|^{2\beta}$ for $T < T_c$, where $\boldsymbol{q}_\parallel$ is the scattering vector component parallel to the surface, $t = (T - T_c)/T_c$ is the reduced temperature and $\boldsymbol{q}_0$ denotes a reciprocal-lattice vector of the superstructure. β is the critical exponent of the order parameter Φ ($\Phi \propto \sqrt{I_0} \propto |t|^\beta$). For $T > T_c$, $I_0 = 0$. The second term describes the contribution of short-

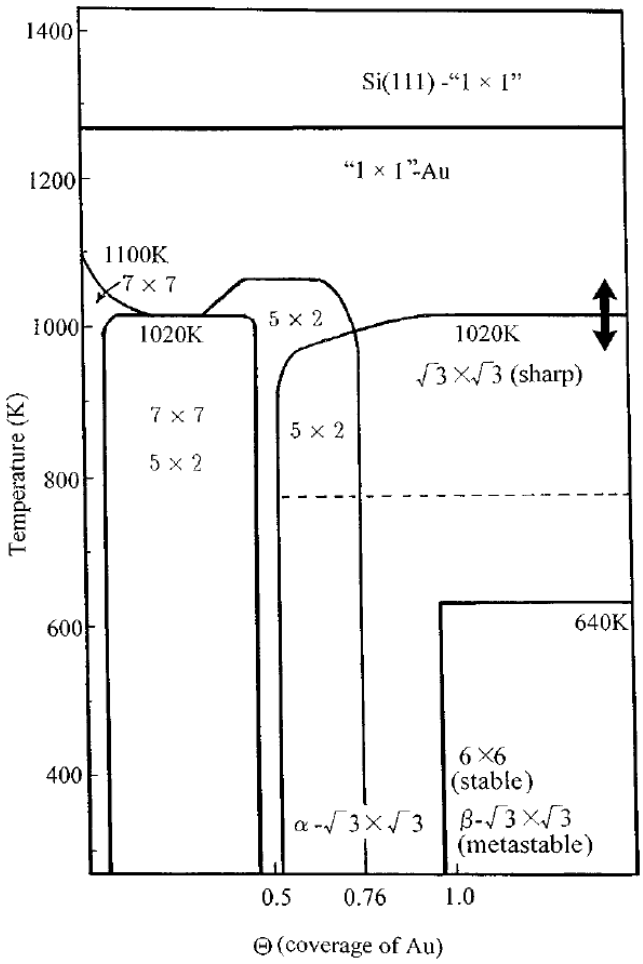

Figure 14. A phase diagram of the Au/Si(111) system based on the RHEED observation as a function of Au coverage (Θ) and temperature [121]. Below $\Theta = 0.76$ ML, a (5×2) pattern coexists with (7×7) or α-$(\sqrt{3} \times \sqrt{3})$R30° patterns. A pure (5×2) pattern appears only in a narrow coverage range around 0.5 ML. Above 0.76 ML, weak reflections in a $(\sqrt{3} \times \sqrt{3})$R30° pattern change their features from α-$(\sqrt{3} \times \sqrt{3})$R30° to β-$(\sqrt{3} \times \sqrt{3})$R30° in a continuous way up to 0.96 ML. At temperatures above 770 K, the weak reflections disappear and only the sharp $(\sqrt{3} \times \sqrt{3})$R30° spots survive. Bold arrows indicate the order–disorder transition reported in [124–127] (from [121, 123]).

range fluctuations of the order parameter (critical scattering). This term is most easily measured above T_c because it is the only remaining term, apart from the background 'bg', the third term. χ_0 (the amplitude of the critical scattering) denotes the susceptibility and ξ the correlation length. For a second-order phase transition they behave as $\chi_0(t) \propto |t|^{-\gamma}$ and $\xi(t) \propto |t|^{-\nu}$. Figure 17 shows the peak intensity for the $(1/3, 1/3)$ superstructure peak, that allows one to determine the value of T_c. The peak intensity of the superstructure beams can be represented versus the reduced temperature t, corrected by the Debye–Waller factor (see figure 18). The plot can be used to determine the critical exponent β of the order parameter by fitting the data with a power law. Other critical exponents can be determined from analogous fits of the experimental

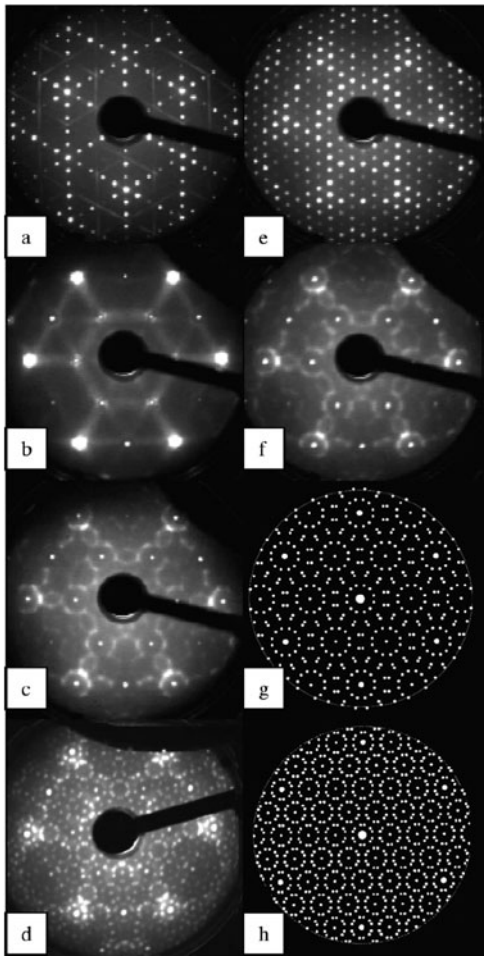

Figure 15. LEED patterns of the Au/Si(111) system as a function of Au coverage Θ at 100 K. (a) $\Theta = 0.5$ ML, (5×2) phase, 98 eV; (b) $\Theta = 0.9$ ML, α-$(\sqrt{3} \times \sqrt{3})$R30° phase, 74 eV; (c) $\Theta = 1.0$ ML, β-$(\sqrt{3} \times \sqrt{3})$R30° phase, 74 eV; (d) $\Theta = 1.0$ ML, $(2\sqrt{21} \times 2\sqrt{21})$ phase, 74 eV; (e) $\Theta = 1.1$ ML, (6×6) phase, 74 eV; (f) $\Theta = 1.1$ ML, quenched β-$(\sqrt{3} \times \sqrt{3})$R30° phase, 74 eV; (g) a schematic LEED pattern of the $(\sqrt{39} \times \sqrt{39})$ phase; (h) a schematic LEED pattern of the $(2\sqrt{21} \times 2\sqrt{21})$ phase. Note that the ring-like diffraction of the β-$(\sqrt{3} \times \sqrt{3})$R30° phase resembles that of a $(\sqrt{39} \times \sqrt{39})$ phase (from [122]).

values of the critical scattering amplitude χ_0 and the correlation length ξ. The results are summarized in table 1, where the experimental values are compared with the predictions of different theoretical models (Ising, three-state Potts, four-state Potts and first order). Note the good agreement with the three-state Potts model. This is in agreement with symmetry arguments applied to a lattice gas, where a continuous order–disorder phase transition of a $(\sqrt{3} \times \sqrt{3})$R30° structure is expected to belong to the three-state Potts universality class [4].

3.2.2. The order–disorder phase transition of the (5 × 1) phase. In the range of Au coverage close to 0.5 ML, a (5×2) phase is observed (see figure 14). Nevertheless, the $2\times$ periodicity of the reconstruction appears as streaks, suggesting a certain degree of disorder in the (5×2)

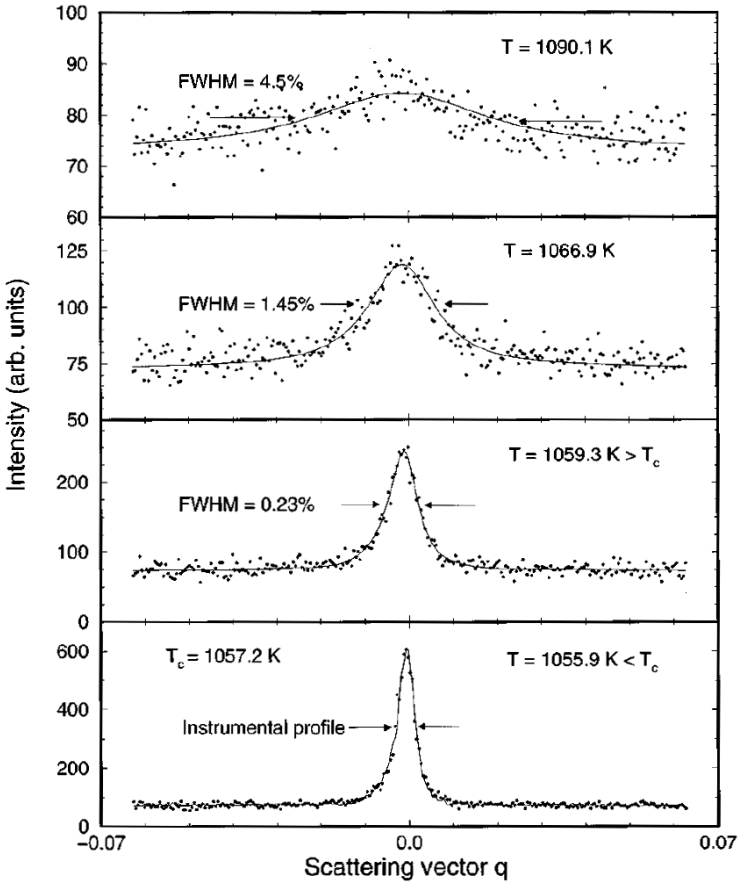

Figure 16. SPA-LEED profiles of the (1/3, 1/3) spot of a Si(111)-β-($\sqrt{3} \times \sqrt{3}$)R30°–Au surface at temperatures below T_c (bottom panel) and above T_c (top three panels). The scattering vector q parallel to the surface and the widths (FWHM) are given in units of k_{10} (from [126]).

Table 1. Experimentally determined critical exponents and comparison with theoretical models, from [126].

	Experiment	Ising	Three-state Potts	Four-state Potts	First order
β	0.113 ± 0.005	0.125	0.111	0.0833	0
ν	0.87 ± 0.07	1	0.833	0.666	0.5
γ	1.35 ± 0.12	1.75	1.44	1.17	1

unit cell or mismatch along the $2\times$ direction (see figure 15). A (5×1) reconstruction can also be observed [127]. The analysis of the phase transition was carried out by using the SPA-LEED technique [127]. The properties depend critically on the coverage in the narrow range of observation of the (5×1) reconstruction. Thus, in the case of low coverage, the temperature dependence of the superstructure spots reveals a commensurate-solid–fluid transition (CFT), while for a slightly higher coverage the phase transition is of the incommensurate-solid–fluid (IFT) type. Note that a continuous transition from an incommensurate (I) solid to a disordered F phase (IFT) belongs to a Kosterlitz–Thouless (KT) universality class [128] while that from a C solid to an I solid (CIT) belongs to a Pokrovsky–Talapov universality

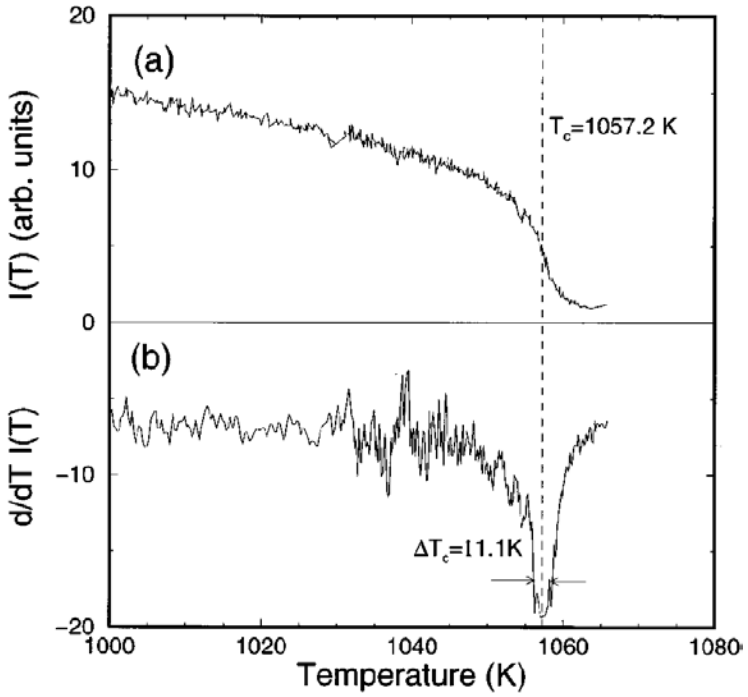

Figure 17. Peak intensity of the (1/3, 1/3) spot of a Si(111)-β-($\sqrt{3}\times\sqrt{3}$)R30°–Au surface versus temperature after Debye–Waller correction. The derivative of (a) with respect to temperature is shown in (b). The minimum in (b), i.e., the inflection point of the curve shown in (a), is an estimate of T_c (from [126]).

class [129]. For a transition from a C solid to a F phase (CFT), the nature of the transition has not been completely understood yet, despite numerous experimental studies [130–132]. The experimentally derived parameters were used to construct the phase diagram shown in figure 19, that is in qualitative agreement with theoretical predictions [133].

3.2.3. The phase transition from α-($\sqrt{3}\times\sqrt{3}$)R30° *to* β-($\sqrt{3}\times\sqrt{3}$)R30° *and* (6×6). A phase transition from α-($\sqrt{3}\times\sqrt{3}$)R30° to β-($\sqrt{3}\times\sqrt{3}$)R30° and (6×6) takes place on changing the coverage (see figure 14) [123]. The continuous change from the α-($\sqrt{3}\times\sqrt{3}$)R30° pattern to β-($\sqrt{3}\times\sqrt{3}$)R30° at RT has been correlated with the increase in domain wall density and their characteristic configuration change as a function of Au coverage in the range $\Theta = 0.76$–0.96. The zigzagging domain walls at $\Theta = 0.79$ at RT are found to transform to roundish ones at 753 K, and finally decompose completely to vanish around 893 K, resulting in apparent large domains of ($\sqrt{3}\times\sqrt{3}$)R30° structure. Above $\Theta = 0.96$, the domain walls are proposed to arrange with a long-range order with (6×6) periodicity when the sample is annealed at around 600 K and slowly cooled. In contrast, a metastable amorphous arrangement in the domain walls with an average separation of $6a$ (where a is the substrate lattice period) is formed after annealing followed by quench cooling, which corresponds to the β-($\sqrt{3}\times\sqrt{3}$)R30°) structure (figure 20).

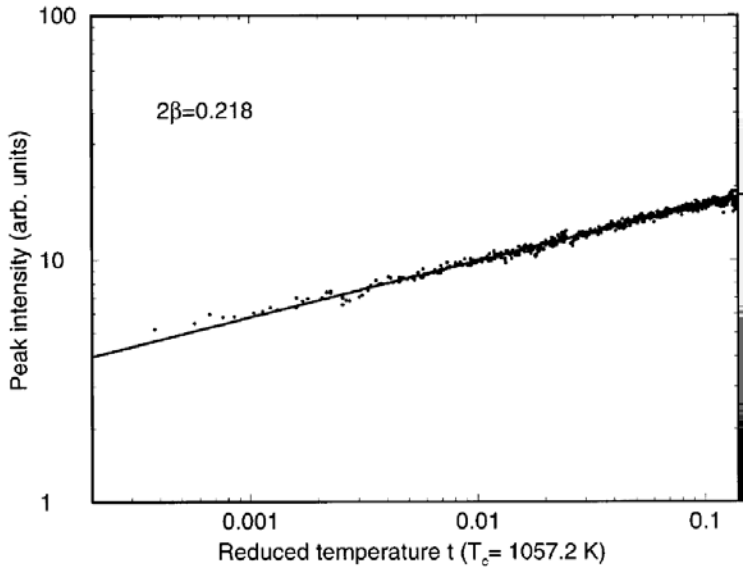

Figure 18. A log–log plot of the peak intensity of a (1/3, 1/3) spot of a Si(111)-β-($\sqrt{3}\times\sqrt{3}$)R30°–Au surface as a function of reduced temperature below T_c. The slope of the fitted power law yields an exponent $2\beta = 0.218$ for this data set (from [126]).

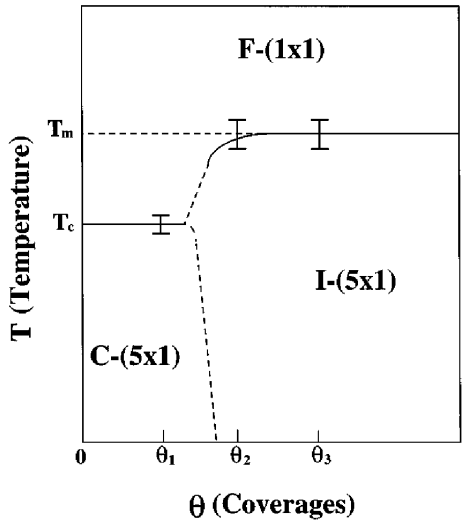

Figure 19. The measured temperature–coverage phase diagram for the Au/Si(111)-(5 × 1) surface. Solid curves represent the second-order transitions with transition temperatures $T_c = 1051 \pm 0.66$ K and $T_m = 1079 \pm 1.5$ K. F denotes a disordered (fluid) phase, C a commensurate-solid phase and I an incomensurate solid phase (from [127]).

3.3. The Si(111)-($\sqrt{3} \times \sqrt{3}$)R30°

The atomic structure of the Si(111)-($\sqrt{3} \times \sqrt{3}$)R30°–Ag surface has been controversial over the last 30 years. Since the first reports [134], almost all surface techniques have been employed to analyse its structure. At the beginning of the 1990s, nine different models

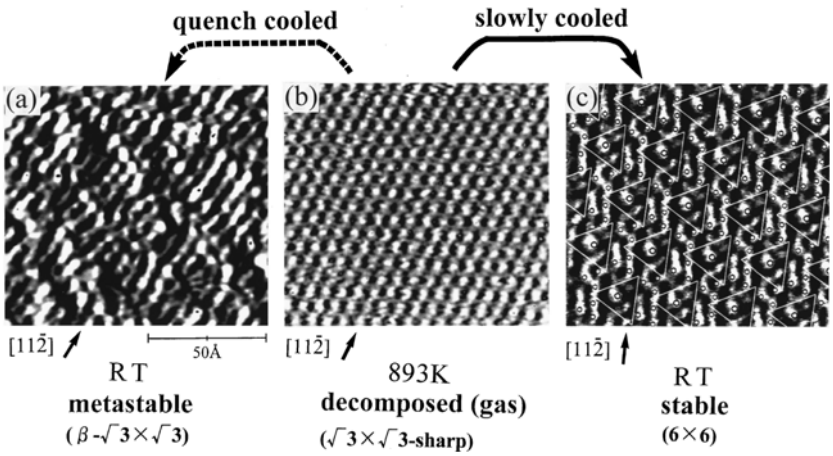

Figure 20. STM images of three different Au/Si(111) structures formed at $\Theta = 1.0$. (a) β-($\sqrt{3} \times \sqrt{3}$)R30° structure prepared by quench cooling after heating at 893 K. (b) ($\sqrt{3} \times \sqrt{3}$)R30° structure at 893 K. (c) (6×6) structure prepared by slow cooling after heating at 893 K (from [123]).

were under discussion: simple honeycomb (HC) [135], missing top layer (MTL) [136], embedded honeycomb (EH) [137], atop trimer (AT) [138], substitutional trimer (ST) [139], centred hexagon (CH) [140], silicon adatom vacancy (SAV) [141], silver honeycomb chained trimer (SHCT) [142] and honeycomb chained triangles (HCT) [143]. Indeed, the situation was such that for almost identical STM images, two independent groups had proposed two different models based on opposite interpretations of the bright protrusions. The first model [144] assumed that the protrusions were due to Ag adatoms, while the second one assigned them to Si atoms [145].

No one of these models was universally accepted until the debate was resolved in favour of the HCT model, on the basis of x-ray diffraction data and low-energy ion scattering [146]. In the structural model it was found that the Ag layer is formed by equilateral triangles built up from adjacent Ag adatoms, sharing apexes with their neighbours (called 'chained triangles'). These same-sized triangles are placed forming a honeycomb arrangement (panel (a) of figure 21). It is important to point out that in the HCT model, Ag atoms are not arranged in a honeycomb network, although this is the structure observed in STM images (panel (a) figure 22). This is because bright protrusions on STM images are only generated by the Ag triangles of the uppermost layer.

The HCT model explained all experimental data obtained up to that moment. However, more recently, theoretical first-principles calculations and STM experiments have reopened the discussion due to the finding of a more stable structure [147]. This new structure (called the 'inequivalent-triangle' model, IET) is obtained by a 6° rotation of the Ag triangles, leading to two different triangle sizes. The structure from the IET model is shown in panel (b) of figure 21.

3.3.1. Electronic structure. Many works have been devoted to the experimental electronic structure of the Si(111)-($\sqrt{3} \times \sqrt{3}$)R30°–Ag surface. Some of them are related to the electronic structure near the Fermi level [148–152].

The Si(111)-($\sqrt{3} \times \sqrt{3}$)R30°–Ag surface exhibits five surface states (labelled S_1–S_5) in the vicinity of the Fermi level [152]. A 2D plot of the electronic structure is shown in figure 23,

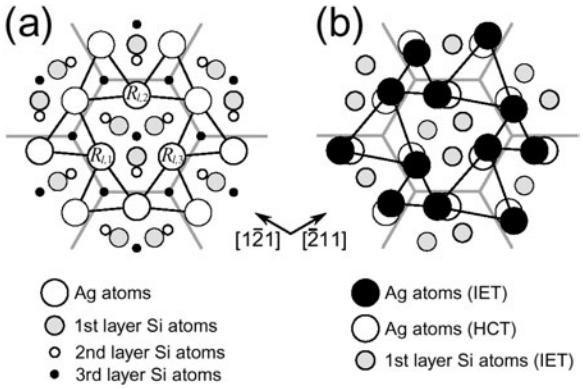

Figure 21. Schematic drawings of the structure of Ag/Si(111)-($\sqrt{3} \times \sqrt{3}$)R30° for the (a) honeycomb chained model (HCT) and (b) inequivalent-triangle model (IET). Black lines indicate Ag triangles (from [157]).

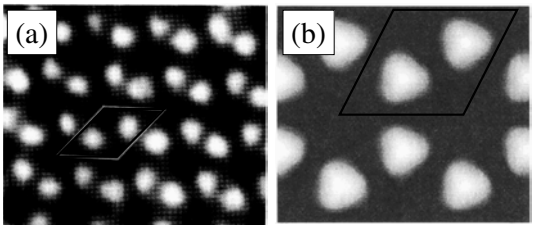

Figure 22. (a) Experimental and (b) theoretical ([153]) STM images of the Ag/Si(111)-($\sqrt{3}\times\sqrt{3}$)R30° surface. The STM topographic image was taken with −1.0 V bias. The theoretical image corresponds to the electronic charge density of unoccupied states 1.5 Å above the Ag layer. The unit cell is also shown (from [145]).

along the two high-symmetry directions $\overline{\Gamma M}$ ([10$\bar{1}$]) and $\overline{\Gamma K}$ ([11$\bar{2}$]) of the hexagonal SBZ. As shown in this figure, the S_1 surface state is half-filled and disperses around the $\bar{\Gamma}$ point. It exhibits the same dispersing behaviour along the $\overline{\Gamma M}$ and $\overline{\Gamma K}$ high-symmetry directions, generating a circular Fermi surface. This suggests a nearly isotropic dispersion, as expected for a 2D nearly-free-electron-like state. Photoemission experiments with different geometric set-ups, as well as theoretical calculations, have determined the Ag 5p nature (with p_x–p_y character) of the S_1 surface band. In the same way, it has been deduced that S_2 and S_5 come from Ag 5s orbitals while S_4, S_1 and S_3 contain mainly Ag $5p_z$ components.

Honeycomb patterns from experimental STM images are easy to explain if one takes into account the electronic structure of the Ag/Si interface. Above the Fermi level, the system is dominated by an empty surface state band (S_1). A calculated 2D plot of this band shows a clear honeycomb arrangement [153], where the maxima of the electronic distribution are in the centre of Ag triangles (see figure 21). This is also consistent with the fact that the best-resolved STM images are obtained under conditions where the electrons tunnel from the tip into empty sample states.

3.3.2. The properties of the surface at low temperature.

(a) *The structural phase transition.* In 1999, Aizawa *et al* [147] reported first-principles theoretical calculations as well as experimental STM images at LT for the Si(111)-($\sqrt{3} \times$

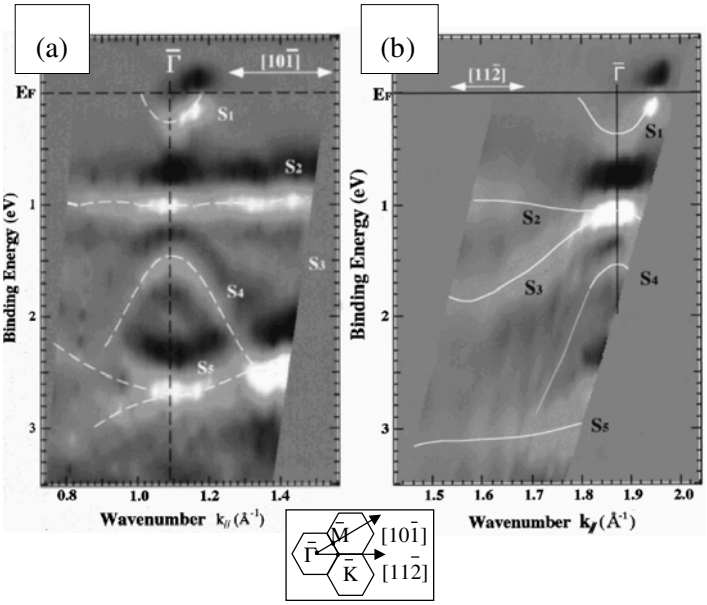

Figure 23. The band structure of Ag/Si(111)-($\sqrt{3} \times \sqrt{3}$)R30° in a greyscale representation, along (a) [10$\bar{1}$] and (b) [11$\bar{2}$] high-symmetry directions. The experiments were done at normal incidence with polarized synchrotron radiation ($h\nu = 21.2$ eV). Lines are a guide to the eye. The inset shows a schematic representation of the surface Brillouin zone (from [152]).

$\sqrt{3}$)R30°–Ag surface. The experiments found the stabilization of a new surface reconstruction at LT, characterized by a hexagonal pattern (at variance with the honeycomb characteristic of the RT structure). From density functional theoretical (DFT) calculations within the local density approximation, they found also a new more stable structure, similar to the HCT model, but with two inequivalent Ag triangles in the unit cell (the IET model). The new structure was 0.1 eV per (($\sqrt{3} \times \sqrt{3}$)R30°) unit cell more stable than the HCT one. The IET optimized structural parameters are nearly the same in the two structures except that the Ag–Ag distances are not identical in the two Ag triangles (3.00 and 3.89 Å in the IET model, versus 3.44 Å in the HCT model). This leads to a broken symmetry where the [11$\bar{2}$] mirror plane disappears (see panel (b) of figure 21). The IET structure can be understood as a rotation of the Ag and Si triangle by 6° in the same direction.

The similarity of the two structures suggests an IET band structure rather similar to the HCT one. However, the bottom of S_1 lies deeper in energy in the IET structure (at $k_{\parallel} = 0$ the binding energy is 0.14 eV while it is only 0.01 eV in the HCT structure). This results in a different charge-density topological distribution of the S_1 surface state in the unit cell. At the $\bar{\Gamma}$ point, it is about three times larger at the centre of the smaller triangles than in the larger triangles. Figure 24 shows a representation of the 2D charge-density plot for the two models. As can be deduced from this figure, STM images should look different in the two cases: the IET structure generates a hexagonal pattern, while the HCT model gives rise to a honeycomb one.

Nevertheless, in spite of these conclusions, most of the STM images of the surface taken at LT exhibit large honeycomb network regions, although a hexagonal pattern is also clearly observed. Two different interpretations are possible: either the theoretical calculations are not precise enough and the HCT is the LT structure, or the surface is the result of time-average

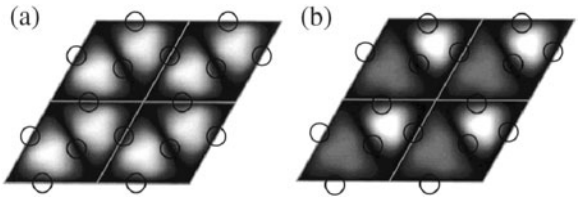

Figure 24. Charge-density plots of the S_1 state with $\vec{k} = 0$ for the (a) HCT and (b) IET models of the Ag/Si(111)-($\sqrt{3} \times \sqrt{3}$)R30° system. The calculation is for a plane 1.7 Å above the Ag layer. Open circles represent Ag-atom positions. Note how the initial hexagonal pattern of the HCT model transforms into a triangular one.

fluctuations of the two rotational IET domains.

In order to investigate this problem, two more detailed theoretical calculations for the LT phase were performed [154, 155]. Although different approximations were used, in both analyses a Monte Carlo simulation (MCS) was applied in order to describe the phase transition. Nakamura *et al* [154] performed MCS with an adiabatic potential representing Ag short-range interactions, and including three-body terms. They concluded that the surface undergoes an order–disorder phase transition. Six different ($\sqrt{3} \times \sqrt{3}$)R30° periodic structures were used. They calculated the energy curves as a function of the Ag displacement from the HCT equivalent positions in each case. Three structures were found to lead to a lower energy, with one, two and three Ag triangle atoms rotated. The last one was the most stable. It was expected that these configurations would dominate in MCS.

Figure 25 represents the theoretical order parameter (Ψ) and specific heat (C_v) as functions of temperature. At high temperatures, Ψ fluctuates around zero, while at ∼250 K it increases rapidly to almost one. This is a clear indication that the system transforms into one IET domain at LT. The peak of C_v at the same temperature means that the phase transition is of second order. From the occupation plot of the system, the results indicate that it is dominated by displaced Ag atoms, instead of Ag in HCT equilibrium positions. As can be observed in figure 26, calculated STM images reveal a hexagonal network. The arrangement of Ag atoms changes from snapshot to snapshot. However, after taking a statistical average, the ordering becomes honeycomb, indicating that this pattern is the result of a time averaging of a fluctuating Ag structure.

In addition to this study, Kakitani *et al* [155] used an order–disorder Hamiltonian as a first simple model to investigate the structural changes of the system. They concluded that the phase transition is of order–disorder type, and the calculated Debye–Waller factor was in good agreement with x-ray diffraction experiments.

(b) *Fluctuations of phase boundaries.* More recently, some more information on the phase transition was gained from LT STM and theoretical studies in regions near a phase boundary [156, 157]. As can be expected for the IET broken [$11\bar{2}$] mirror plane symmetry, the experiments reveal two types of twin domain, and different types of boundary appear between them. A honeycomb pattern is observed in standard out-of-phase domains, separating regions with hexagonal patterns. The theoretical calculations considered explicitly the Ag thermal motion [157]. It was found that the HCT structure observed comes from the fluctuating boundary of IET domains. The honeycomb pattern appears in regions where the probabilities for each site to be in one IET domain and in the neighbour are nearly the same on average. The surface was confirmed to undergo an order–disorder phase transition, and the STM images were well understood as averages for a disordered state.

In summary, the Si(111)-($\sqrt{3} \times \sqrt{3}$)R30°–Ag surface undergoes an structural order–disorder phase transition from a honeycomb to a hexagonal pattern upon decreasing the

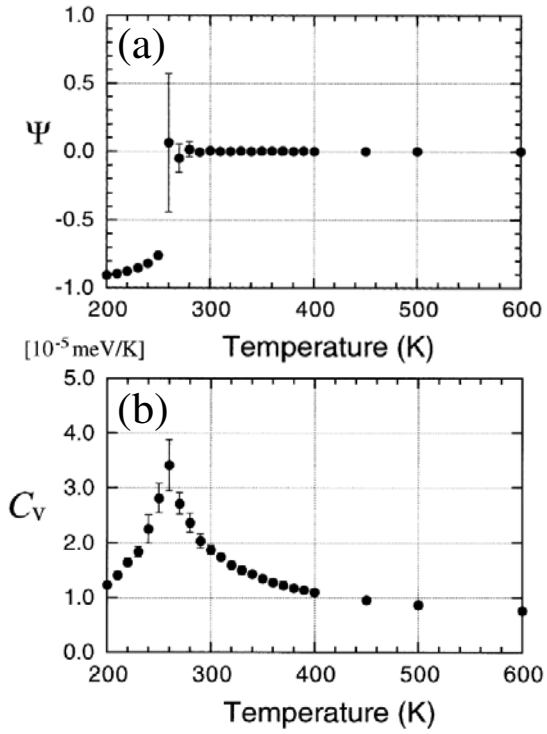

Figure 25. Temperature dependences of the long-range order parameter Ψ (a) and the specific heat C_v (b) for the Ag/Si(111)-($\sqrt{3} \times \sqrt{3}$)R30° system (from [154]).

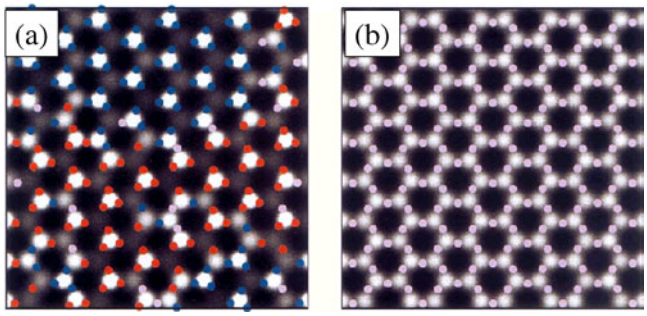

Figure 26. Calculated STM images at 300 K for the Ag/Si(111)-($\sqrt{3} \times \sqrt{3}$)R30° surface. (a) represents one snapshot, while (b) represents a time average of the same area. The (coloured as follows in the electronic version, monochrome in printed version) small circles indicate the positions of Ag atoms: red for $u \geqslant 0.25$, blue for $u \leqslant -0.25$ and purple for $|u| < 0.25$ respectively, the displacement from the HCT positions being u (from [154]).

temperature. The RT honeycomb network observed in STM images has been interpreted as the result of time averaging of different possible IET structures. This result is also supported by the theoretical behaviour of the order parameter and the specific heat as a function of the temperature. Although theoretical calculations indicate clearly the order–disorder nature of the phase transition, more experimental results are needed in order to definitively confirm this assignment.

Finally, this phase transition analysis gives a warning of the tendency to relate STM images to motionless and stable structures. This tendency is stronger at LT, because thermal fluctuations become hardly to be expected. However, the fluctuations of the Si(111)-$(\sqrt{3} \times \sqrt{3})$R30°–Ag surface are too fast to be detected by a dynamic STM amplifier.

4. Conclusions

The analysis of reversible phase transitions in semiconductor surfaces has been a fertile research field for several decades. The improvements in experimental and theoretical methods during recent years have made it possible to analyse phase transitions with a precision that could not be imagined a decade ago. Research at temperatures much lower than reached before have also opened up a new world of stable structures, and the role of thermal fluctuations appears to be much more important than expected in many apparently static structures. For all these reasons, renewed interest in these areas can be foreseen for the near future.

Acknowledgments

We acknowledge financial support by MCyT (Spain) under grant BFM-2001-0244 and by Comunidad de Madrid (Spain) under grant 07N/0056/2001.

References

[1] Bauer E 1987 *Structure and Dynamics of Surfaces II (Springer Topics in Current Physics vol 43)* ed V Schommers and P von Blanckenhagen (Berlin: Springer)
[2] Binder K and Landau D 1989 *Molecule–Surface Interaction* ed K Lawley (New York: Wiley)
[3] Persson B N J 1992 *Surf. Sci. Rep.* **15** 1
[4] Schick M 1981 *Prog. Surf. Sci.* **11** 245
[5] Matthews-Morgan D, Landau D P and Swendsen H 1984 *Phys. Rev. Lett.* **53** 679
[6] Novotny M and Landau D 1985 *Phys. Rev.* B **32** 3112
[7] Chen S, Ferrenberg A M and Landau D P 1992 *Phys. Rev. Lett.* **69** 1213
[8] Sokolowski M and Pfnür H 1989 *Phys. Rev. Lett.* **63** 183
[9] Duke C B 1996 *Chem. Rev.* **96** 1237 and references therein
[10] Kubby J A and Boland J J 1996 *Surf. Sci. Rep.* **26** 63 and references therein
[11] Mönch W 1993 *Semiconductor Surfaces and Interfaces* (Berlin: Springer) and references therein
[12] LaFemina J P 1992 *Surf. Sci. Rep.* **16** 133 and references therein
[13] Wolkow R A 1992 *Phys. Rev. Lett.* **68** 2636
[14] Aristov V Yu, Douillard L, Fauchoux O and Soukiassian P 1997 *Phys. Rev. Lett.* **79** 3700
[15] Johnson A D *et al* 1991 *Phys. Rev.* B **44** 1134
[16] Kevan S D and Stoffel N G 1984 *Phys. Rev. Lett.* **53** 702
[17] Kevan S D 1985 *Phys. Rev.* B **32** 2344
[18] Takeuchi N, Selloni A and Tosatti E 1994 *Phys. Rev. Lett.* **72** 2227
[19] Modesti S, Dhanak V R, Sancrotti M, Santoni A, Persson B N J and Tosatti E 1994 *Phys. Rev. Lett.* **73** 1951
[20] Farias D, Lange G, Rieder K-H and Toennies J P 1997 *Phys. Rev.* B **55** 7023
[21] Glebov A L, Toennies J P and Vollmer S 1999 *Phys. Rev. Lett.* **82** 3300
[22] Stumpf R and Marcus P M 1993 *Phys. Rev.* B **47** 16 016
[23] Meli C A, Greene E F, Lange G and Toennies J P 1995 *Phys. Rev. Lett.* **74** 2054
[24] Johnson A D, Norris C, Frenken J W M, MacDonald J E, Van Silfhout R G and Van Der Veen J F 1991 *Phys. Rev.* B **44** 1134
[25] Ihm J, Lee D H, Joannopoulos J D and Xiong J J 1983 *Phys. Rev. Lett.* **51** 1872
[26] Landemark E, Karlsson C J, Chao Y-C and Uhrberg R I G 1992 *Phys. Rev. Lett.* **69** 1588
[27] Shkrebtii A I and Del Sole R 1993 *Phys. Rev. Lett.* **70** 2645
[28] Fontes E, Patel J R and Comin F 1993 *Phys. Rev. Lett.* **70** 2790
[29] Hamers R J, Tromp R M and Demuth J E 1986 *Phys. Rev.* B **34** 5343
[30] Wiesendanger R, Bürgler D, Tarrach G and Güntherodt H-J 1990 *Surf. Sci.* **232** 1

[31] Johansson L S O, Uhrberg R I G, Mårtensson P and Hansson G V 1990 *Phys. Rev.* B **42** 1305
[32] Chadi D J 1979 *Phys. Rev. Lett.* **43** 43
[33] Roberts N and Needs R J 1990 *Surf. Sci.* **239** 112
[34] Tabata T, Aruga T and Murata Y 1987 *Surf. Sci. Lett.* **179** L63
[35] Kondo Y, Amakusa T, Iwatsuki M and Tokumoto H 2000 *Surf. Sci.* **453** L318
[36] Yokoyama T and Takayanagi K 2000 *Phys. Rev.* B **61** R5078
[37] Inoue K, Morikawa Y, Terakura K and Nakayama M 1994 *Phys. Rev.* B **49** 14 774
[38] Ramstad A, Brocks G and Kelly P J 1995 *Phys. Rev.* B **51** 14 504
[39] Fritsch J and Pavone P 1995 *Surf. Sci.* **344** 159
[40] Northrup J E 1993 *Phys. Rev.* B **47** 10 032
[41] Shigekawa H, Hata K, Miyake K, Ishida M and Ozawa S 1997 *Phys. Rev.* B **55** 15 448 and references therein
[42] Krüger P and Pollmann J 1995 *Phys. Rev. Lett.* **74** 1155
[43] Needels M, Payne M C and Joannopoulos J D 1987 *Phys. Rev.* B **58** 1765
[44] Shkrebtii A I, Di Felice R, Bertoni C M and Del Sole R 1993 *Phys. Rev.* B **51** 11 201
[45] Saxena A, Gawlinski E T and Gunton J D 1985 *Surf. Sci.* **160** 618
[46] Lucas C A, Dower C S, McMorrow D F, Wong G C L, Lamelas F J and Fuoss P H 1993 *Phys. Rev.* B **47** 10 375
[47] Kubota M and Murata Y 1994 *Phys. Rev.* B **49** 4810
[48] Imry Y and Ma S-K 1975 *Phys. Rev. Lett.* **35** 1399
[49] Landau D P 1976 *Phys. Rev.* B **13** 2997
[50] Cvetko D, Floreano L, Crottini A, Morgante A and Tommasini F 2000 *Surf. Sci.* **447** L147
[51] Zandvliet H J W, Caspers W J and van Silfhout A 1991 *Solid State Commun.* **78** 455
[52] Alvarez J, Etgens V H, Torrelles X, van der Vegt H A, Fajardo P and Ferrer S 1996 *Phys. Rev.* B **54** 5581
[53] Nakamura Y, Kawai H and Nakayama M 1997 *Phys. Rev.* B **55** 10 549
[54] Tosatti E 1978 *Solid State Commun.* **25** 637
[55] Takayanagi K, Tanishiro Y, Takahashi M and Takahashi S 1985 *J. Vac. Sci. Technol.* A **3** 1502
Takayanagi K, Tanishiro Y, Takahashi M and Takahashi S 1985 *Surf. Sci.* **164** 367
[56] Lander J J 1964 *Surf. Sci.* **1** 125
[57] Ino S 1977 *Japan. J. Appl. Phys.* **16** 891
[58] Bennett P A and Webb M W 1981 *Surf. Sci.* **104** 74
[59] Osakabe N, Tanishiro Y, Yagi K and Honjo G 1981 *Surf. Sci.* **109** 353
[60] McRae E G and Malic R A 1985 *Surf. Sci.* **161** 25
[61] Kohmoto S and Ichimiya A 1989 *Surf. Sci.* **223** 400
[62] Hasegawa S, Nagai Y, Oonishi T and Ino S 1993 *Phys. Rev.* B **47** 9903
[63] Chevrier J, Vinh L T and Cruz A 1992 *Surf. Sci.* **268** L261
[64] Landau L D and Lifshitz E M 1980 *Course of Theoretical Physics* vol 5 (London: Pergamon)
[65] Blandin A 1973 *Phys. Lett.* A **45** 275
[66] Zangwill A 1988 *Physics at Surfaces* (Cambridge: Cambridge University Press) p 113
[67] Latyshev A V *et al* 1991 *Surf. Sci.* **254** 90
[68] Telieps W and Bauer E 1985 *Surf. Sci.* **162** 163
[69] Phaneuf J *et al* 1992 *Surf. Sci.* **268** 227
[70] Miki K *et al* 1992 *Ultramicroscopy* **42–44** 851
[71] Suzuki T and Hirabayashi Y 1993 *OSA Tech. Dig. Ser.* **12** 141
Suzuki T and Hirabayashi Y 1993 *Japan. J. Appl. Phys.* **32** L610
[72] Höfer U, Li Leping, Ratzlaff G A and Heinz T F 1995 *Phys. Rev.* B **52** 5264
[73] Iwasaki H *et al* 1987 *J. Phys. Soc. Japan* **56** 3425
[74] Ha J S and Greene E F 1989 *J. Chem. Phys.* **91** 571
[75] Kitamura S, Sato T and Iwatsuki M 1991 *Nature* **351** 215
[76] Suzuki M *et al* 1993 *Japan. J. Appl. Phys.* **32** 3247
[77] Phaneuf J *et al* 1993 *Phys. Rev. Lett.* **71** 2284
[78] Yang Y-N and Williams E D 1994 *Phys. Rev. Lett.* **72** 1862
[79] Sakamoto Y and Kanamori J 1993 *J. Phys. Soc. Japan* **62** 563
[80] Fukaya Y and Shigeta Y 2000 *Phys. Rev. Lett.* **85** 5150
[81] Becker R S, Golovchenko J A and Swartzentruber B S 1985 *Phys. Rev. Lett.* **54** 2678
[82] Becker R S, Swartzentruber B S, Vickers J S and Klitsner T 1989 *Phys. Rev.* B **39** 1663
[83] Phaneuf R J and Webb M B 1985 *Surf. Sci.* **164** 167
[84] Feidenhans'l R, Pedersen J S, Bohr J, Nielsen A, Grey F and Johnson R L 1988 *Phys. Rev.* B **38** 9715
[85] Feenstra R M, Slavin A J, Held G A and Lutz M A 1991 *Phys. Rev. Lett.* **66** 3257
Feenstra R M and Slavin A J 1991 *Surf. Sci.* **251–2** 401

[86] Aarts J, Hoeven A-J and Larsen P K 1988 *Phys. Rev.* B **38** 3925
[87] Hricovini K, Le Lay G, Abraham M and Bonnet J E 1990 *Phys. Rev.* B **41** 1258
[88] Abraham M, Le Lay G and Hila J 1990 *Phys. Rev.* B **41** 9828
[89] Zeng X, El-Kholy I and Elsayed-Ali H 1999 *Phys. Rev.* B **59** 14 907
[90] Goldoni A *et al* 1997 *Surf. Sci.* **382** 336
[91] van der Gon A W *et al* 1991 *Surf. Sci.* **241** 335
[92] Modesti S and Santoni A 1989 *Solid State Commun.* **72** 315
[93] Chen X-J, Levi A C and Tosatti E 1991 *Nuovo Cimento Soc. Ital. Fis.* D **13** 919
[94] Glebov A L, Toennies J P and Vollmer S 1999 *Phys. Rev. Lett.* **82** 3300
[95] Mak A *et al* 1991 *Phys. Rev. Lett.* **66** 2002
[96] Pasquali L, Nannarone S, Canepa M and Mattera L 1998 *Phys. Rev.* B **57** 2507
[97] Gai Z, Yu H and Yang W S 1996 *Phys. Rev.* B **53** 13 547
[98] Choyke W J, Matsunami H M and Pensl G (ed) 1998 *Silicon Carbide: a Review of Fundamental Questions and Applications to Current Device Technology* vol 1 and 2 (Berlin: Akademie)
[99] Johansson L S O, Duda L, Laurenzis M, Krieftewirth M and Reihl B 2000 *Surf. Sci.* **445** 10
[100] Derycke V, Soukiassian P, Mayne A, Dujardin G and Gautier J 1998 *Phys. Rev. Lett.* **81** 5868
[101] Soukiassian P, Semond F, Mayne A and Dujardin G 1997 *Phys. Rev. Lett.* **79** 2498
[102] Soukiassian P, Semond F, Douillard L, Mayne A, Dujardin G, Pizzagalli L and Joachim C 1997 *Phys. Rev. Lett.* **78** 907
[103] Shek M L 1996 *Surf. Sci.* **349** 317
[104] Aristov V Y, Douillard L, Fauchoux O and Soukiassian P 1997 *Phys. Rev. Lett.* **79** 3700
[105] Catellani A, Galli G and Gygi F 1996 *Phys. Rev. Lett.* **77** 5090
[106] Enriquez H, Derycke V, Aristov V Yu, Soukiassian P, Le Lay G, di Cioccio L, Cricenti A, Croti C, Ferrari L and Perfetti P 2000 *Appl. Surf. Sci.* **162–3** 559
[107] Soukiassian P 1999 *Mater. Sci. Eng.* B **61** 506 and references therein
[108] Carpinelli J M, Weitering H H, Plummer E W and Stumpf R 1996 *Nature* **381** 398
[109] Carpinelli J M, Weitering H H, Bartkowiak M, Stumpf R and Plummer E W 1997 *Phys. Rev. Lett.* **79** 2859
[110] Custance O *et al* 2002 at press
[111] Debe M K and King D A 1977 *J. Phys. C: Solid State Phys.* **10** L303
Felter T E *et al* 1977 *Phys. Rev. Lett.* **38** 1138
Wang X W and Weber W 1987 *Phys. Rev. Lett.* **58** 1452
Smith K E *et al* 1990 *Phys. Rev.* B **42** 5385
Hoffman F M *et al* 1994 *Phys. Rev. Lett.* **72** 1256
[112] Avila J *et al* 1999 *Phys. Rev. Lett.* **82** 442
[113] Mascaraque A, Avila J, Alvarez J, Asensio M C, Ferrer S and Michel E G 1999 *Phys. Rev. Lett.* **82** 2524
[114] Mascaraque A, Avila J, Michel E G and Asensio M C 1998 *Phys. Rev.* B **57** 14 758
[115] Uhrberg R I G and Balasubramanian T 1998 *Phys. Rev. Lett.* **81** 2108
[116] Melechko A V *et al* 1999 *Phys. Rev. Lett.* **83** 999
Melechko A V *et al* 2000 *Phys. Rev.* B **61** 2235
[117] Melechko A V *et al* 2001 *Phys. Rev.* B **64** 235424
[118] Floreano L *et al* 2001 *Phys. Rev.* **64** 075405
[119] Pérez R, Ortega J E and Flores F 2001 *Phys. Rev. Lett.* **86** 4891
[120] Ortega J, Perez R and Flores F 2002 *J. Phys.: Condens. Matter* **14** 7979
[121] Ino S 1988 *Reflection High Energy Electron Diffraction and Reflection Electron Imaging of Surfaces* ed P K Larsen and P J Dobson (New York: Plenum)
Ino S 1982 *J. Phys. Soc. Japan* **37** 82 (in Japanese)
[122] Zhang H M, Balasubramanian T and Uhrberg R I G 2001 *Phys. Rev.* B **65** 035314
[123] Nagao T, Hasegawa S, Tsuchie K, Ino S, Voges C, Klos G, Pfnür H and Henzler M 1998 *Phys. Rev.* B **57** 10 100
[124] Hasegawa S, Nagai Y, Oonishi T and Ino S 1993 *Phys. Rev.* B **47** 9903
[125] Hasegawa S, Nagai Y, Oonishi T, Kobayashi N, Miyake T, Murakami S, Ishii Y, Hanawa D and Ino S 1994 *Phase Transit.* **53** 87
[126] Nakajima Y, Voges C, Nagao T, Klos G, Pfnür H and Hasegawa S 1997 *Phys. Rev.* B **55** 8129
[127] Hong J S, Kim H W, Kim H J and Chung J W 1996 *Phys. Rev.* B **55** 7047
[128] Kosterlitz J M and Thouless D J 1972 *J. Phys. C: Solid State Phys.* **5** L124
[129] Pokrovsky V L and Talapov A L 1979 *Phys. Rev. Lett.* **42** 65
[130] Campuzano J C *et al* 1985 *Phys. Rev. Lett.* **54** 2684
[131] Schreiner J, Jacobi K and Selke W 1994 *Phys. Rev.* B **49** 2706

[132] Abernathy D L, Song S, Blum K I, Birgeneau R J and Mochrie S G 1994 *Phys. Rev.* B **49** 2691
[133] Schulz H J 1983 *Phys. Rev.* B **28** 2746
[134] Spiegel K 1967 *Surf. Sci.* **7** 125
[135] Le Lay G 1983 *Surf. Sci.* **132** 169
Aono M, Souda R, Oshima C and Oshizawa Y 1986 *Surf. Sci.* **168** 713
Wilson R J and Chiang S 1987 *Phys. Rev. Lett.* **59** 2329
Wilson R J and Chiang S 1987 *Phys. Rev. Lett.* **58** 369
[136] Bullok E L, Herman G S, Yamada M, Friedman D J and Fadley C S 1990 *Phys. Rev.* B **41** 1703
Kono S, Higashiyama K and Sakawa T 1986 *Surf. Sci.* **165** 21
Kono S, Sakurai H, Higashiyama K and Sakawa T 1983 *Surf. Sci.* **130** L299
Kono S, Higashiyama K, Kinoshita T, Miyahara T, Kato H, Oshawa H, Enta Y, Maeda F and Yaegashi Y 1987 *Phys. Rev. Lett.* **58** 1555
[137] Saitoh M, Shoji F, Oura K and Hanawa T 1981 *Surf. Sci.* **112** 306
Terada Y, Yoshizauka T, Oura K and Hanawa T 1982 *Surf. Sci.* **114** 65
Söhr J, Jaeger R, Rossi G, Kendelewic T and Lindau I 1983 *Surf. Sci.* **134** 813
[138] Wehking F, Beckermann H and Niedermayer R 1978 *Surf. Sci.* **71** 364
[139] Horio Y and Ichimiya A 1985 *Surf. Sci.* **164** 589
Chang C S, Porter T L and Tsong I S T 1988 *J. Vac. Sci. Technol.* B **3** 1906
Porter T L, Chang C S and Tsong I S T 1988 *Phys. Rev. Lett.* **60** 1739
Horio Y and Ichimiya A 1983 *Surf. Sci.* **133** 393
Demuth J E, Van Loenen E J, Tromp R M and Hamers R J 1988 *J. Vac. Sci. Technol.* B **6** 18
Van Loenen E J, Demuth J E, Tromp R M and Hamers R J 1987 *Phys. Rev. Lett.* **58** 373
[140] Le Lay G, Chauvet A, Manneville M and Kern R 1981 *Surf. Sci.* **9** 190
[141] Copel M and Tromp R M 1989 *Phys. Rev.* B **39** 12 688
[142] Vlieg E, van der Gon A W, van der Veen J F, MacDonald J E and Norris C 1989 *Surf. Sci.* **209** 100
[143] Takahashi T, Nakatani S, Okamoto N, Ichikawa T and Kikuta S 1988 *Japan. J. Appl. Phys.* **27** L753
Ichimiya A, Kohmoto S, Fujii T and Horio Y 1989 *Appl. Surf. Sci.* **41/42** 82
Williams R S, Daley R S, Huang J H and Charatan R M 1988 *Appl. Surf. Sci.* **41–2** 70
Daley R S, Charatan R M and Williams R S 1990 *Surf. Sci.* **240** 136
Takahashi T 1989 *Proc. Workshop on the Si(111)/Ag Surface* unpublished
[144] Wilson R J and Chiang S 1987 *Phys. Rev. Lett.* **58** 369
[145] van Loenen E J, Demuth J E, Tromp R M and Hamers R J 1987 *Phys. Rev. Lett.* **58** 373
[146] Takahashi T *et al* 1988 *Japan. J. Appl. Phys.* **27** L753
Katayama M, Williams R S, Kato M, Nomura E and Aono M 1991 *Phys. Rev. Lett.* **66** 2762
Ding Y G, Chan C T and Ho K M 1991 *Phys. Rev. Lett.* **67** 1454
Takahashi T *et al* 1991 *Surf. Sci.* **242** 54
[147] Aizawa H, Tsukada M, Sato N and Hasegawa S 1999 *Surf. Sci.* **429** L509
[148] Hansson G V, Bachrach R Z, Bauer R S and Chiaradia P 1981 *Phys. Rev. Lett.* **46** 1033
[149] Houzay F *et al* 1983 *Surf. Sci.* **124** L1
[150] Yokutsuka T *et al* 1983 *Surf. Sci.* **127** 35
[151] Johansson L S O, Landemark E, Karlsson C J and Uhrberg R I G 1989 *Phys. Rev. Lett.* **63** 2092
[152] Tong X, Ohuchi S, Sato N, Tanikawa T, Nagao T, Matsuda I, Aoyagi Y and Hasegawa S 2001 *Phys. Rev.* B **64** 205316
[153] Ding Y G, Chan C T and Ho K M 1991 *Phys. Rev. Lett.* **67** 1454
[154] Nakamura Y, Kondo Y, Nakamura J and Watanabe S 2001 *Surf. Sci.* **493** 206
[155] Kakitani K, Yoshimori A, Aizawa H and Tsukada M 2001 *Surf. Sci.* **493** 200
[156] Sato N, Nagao T and Hasegawa S 1999 *Surf. Sci.* **442** 65
[157] Nakamura Y, Kondo Y, Najamura J and Watanabe S 2001 *Phys. Rev. Lett.* **87** 156102